**UNIVERSITÀ DEGLI STUDI DELLA TUSCIA DI VITERBO**

**DIPARTIMENTO DI SCIENZE ECOLOGICHE E BIOLOGICHE**

**Corso di Dottorato di Ricerca in**

Genetica e Biologia Cellulare - XXVIII Ciclo.

# THE KINASE HIPK2 REGULATES CYTOKINESIS THROUGH THE MICROTUBULE SEVERING SPASTIN

**s.s.d. BIO/11**

**Tesi di dottorato di**:

Dott.ssa Loredana Biancolillo

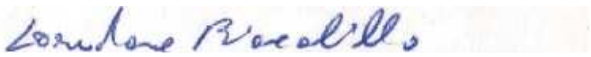

**Coordinatore del corso**

Prof. Giorgio Prantera

**Tutore**

Dott.ssa Cinzia Rinaldo

**06.05.2016**

# INDEX

# ABSTRACT

The oncosuppressor HIPK2 is a kinase involved in the cell fate decisions in the development and response to stress. Recently, it was demonstrated the relevance of this kinase in the control of cytokinesis and prevention of chromosomal instability (CIN). HIPK2 is required for cytokinesis and prevents tetraploidization by phosphorylating the extra-chromosomal histone H2B at the midbody, the organelle-like structure formed at the cleavage furrow between the two daughter cells (Rinaldo et al., 2012). HIPK2-depleted cells do not successfully complete cytokinesis, leading to polyploidization, CIN, and increased tumorigenicity (Valente et al., 2015).

To get hints on the mechanism through which HIPK2 controls cytokinesis, we have investigated the interplay between HIPK2 and crucial cytokinesis factors by analyzing their epistatic localization relationships at midbody in HIPK2-depleted cells (H-i).

Our results show that HIPK2 depletion does not affect the localization of proteins involved in midbody formation/stabilization (i.e. CPC proteins, PLK1, MKLP1, MgcRacGAP1, PRC1, ECT2 and citron Kinase), while strongly affects the localization of the microtubule severing protein spastin, whose activity is required for abscission, the final step of cytokinesis. Spastin could not be detected at the midbody in a high percentage (37±4.9%) of H-i cells. Spastin possesses microtubule (MT)-severing ability and contributes to different processes involving MT/cytoskeleton, such as cytokinesis, membrane modelling, intracellular and axonal vesicle transports (Trotta et al., 2004; Connell et al., 2009). Interestingly, we noticed that H-i cells show cytokinesis defects strongly resembling those of spastin-depleted cells and spastin over-expression rescues H-i cytokinesis defects, but not H2B phosphorylation at the midbody, indicating that the two events are independent. A biochemical characterization of the HIPK2/spastin cross-talk showed that HIPK2 directly regulates spastin levels in a phosphorylation-dependent manner. In particular, HIPK2 phosphorylates spastin at S268 in vitro and this phosphorylation is required for spastin stability. Notably, we observed that over-expression of a phosphomimetic spastin S268D mutant, but not non-phosphorylatable S268A mutant, rescues cytokinesis defects in H-i cells. Overall, these findings support the idea that HIPK2-mediated phosphorylation of spastin contributes to reach the spastin dosage required for abscission.

# INTRODUCTION

## 1 Cytokinesis and its molecular control

Cytokinesis follows mitosis (Fig. 1), partly overlaps with it and completes the cell division. Cytokinesis is usually divided in four stages: central spindle (midzone) assembly, cleavage furrow ingression, midbody formation and abscission (Fig. 2; Chen et al., 2012).

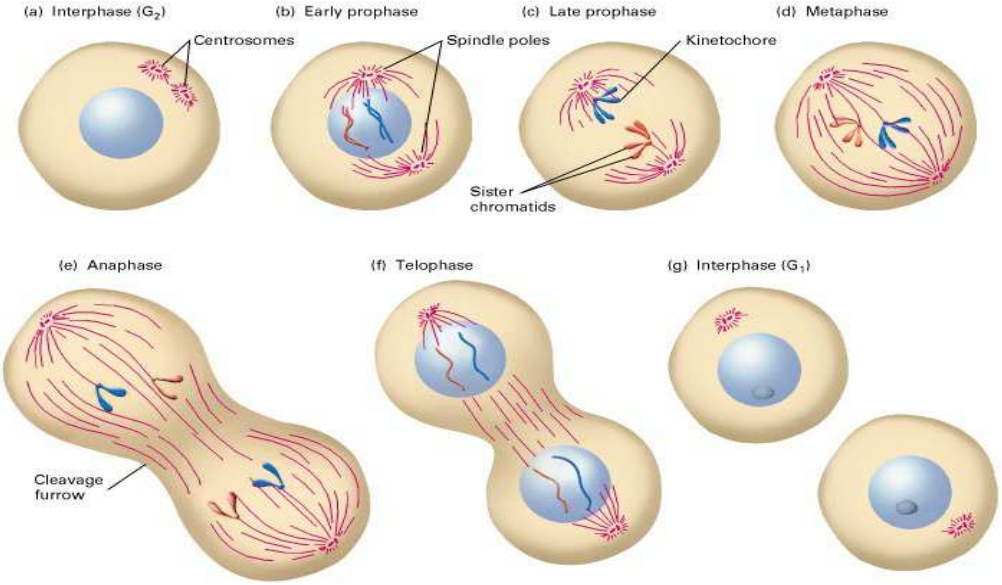


**Figure 1. The stages of mitosis in an animal cell.**
The eukaryotic cells ensure the faithful segregation of sister chromatids and the proper maintenance of genome stability through mitosis. (a) Interphase: The G2 stage of interphase immediately precedes the beginning of mitosis and follows chromosomal DNA replication during the S phase. The chromosomes, each containing a sister chromatid, are still dispersed and not visible as distinct structures. During interphase, the centrioles are replicated, forming small daughter centrioles. (b) Early prophase: The centrosomes, each with a daughter centriole, begin moving toward opposite poles of the cell. The chromosomes can be seen as long threads, and the nuclear membrane begins to disaggregate into small vesicles. (c) Prophase: Chromosome condensation is completed; each visible chromosome structure is composed of two chromatids held together at their centromeres. The microtubular spindle fibres begin to radiate from the regions just adjacent to the centrosomes. Some spindle fibers reach from pole to pole; most go to chromatids and attach at kinetochores. (d) Metaphase: The chromosomes move toward the equator of the cell, where they become aligned in the equatorial plane. (e) Anaphase: The two sister chromatids separate into independent chromosomes. Each contains a centromere that is linked by a spindle fiber to one pole, to which it moves. Simultaneously, the cell elongates, as do the pole-to-pole spindles. Cytokinesis begins as the cleavage furrow starts to form. (f) Telophase: New nuclear membranes form around the daughter nuclei; the chromosomes uncoil and become less distinct; the nucleolus becomes visible again. Cytokinesis is nearly complete, and the spindle disappears as the MTs and other fibers depolymerize. Throughout mitosis the “daughter” centriole at each pole grows, so that by telophase each of the emerging daughter cells has two full-length centrioles. Upon the completion of cytokinesis, each daughter cell enters the G1 phase of the cell cycle and proceeds again around the cycle. (Molecular Cell Biology. 4th edition. Lodish H, Berk A, Zipursky SL, et al. New York: W. H. Freeman; 2000.)

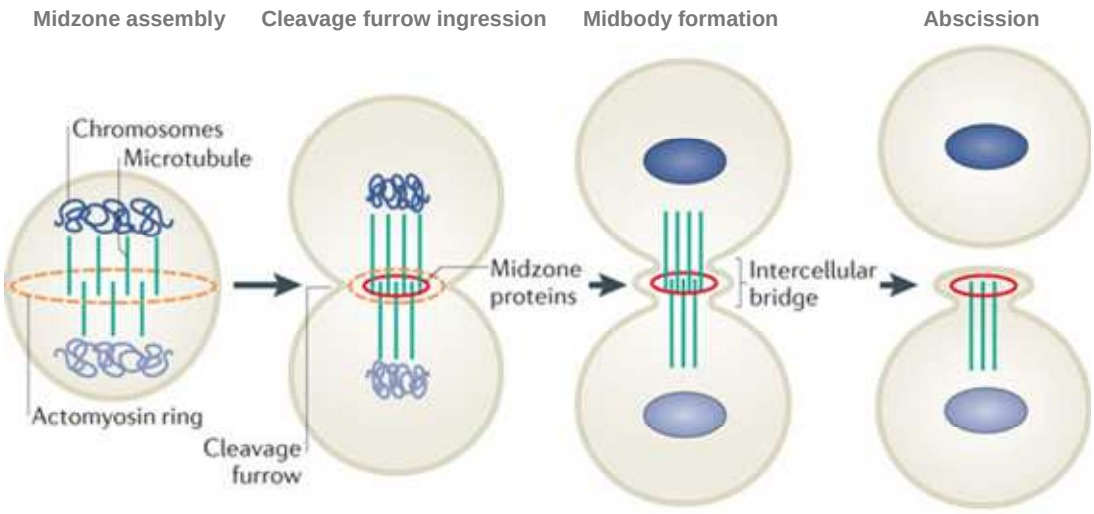


**Figure 2. The four stages of cytokinesis.**
Following entry into cytokinesis, the actomyosin ring and antiparallel midzone MTs form between the segregated chromosomes. In early cytokinesis, midzone MTs gradually compact through the crosslinking of associated midzone proteins, and the cleavage furrow narrows. After furrowing, the intercellular bridge (midbody) with the compacted MTs connects the two daughter cells. The midbody contains overlapping MTs, the midbody ring (derived from crosslinked midzone proteins) and amorphous, electron-dense material. Abscission occurs adjacent to the midbody by multiple pathways that orchestrate severing of the intercellular bridge. In certain cell types, a second bridge-severing event occurs on the other side of the bridge (Modified by Chen et al., 2012).

This process is finely regulated and drove by mitotic spindle MTs and the spindle midzone. At the center of the spindle midzone, actin filaments with motor protein myosin II and other proteins assemble a contractile ring that bisects the dividing cell. The position of the division plane and the formation of the ring are established by two populations of MTs: astral and central spindle MTs, after the sister chromatids move towards the two opposite spindle poles in anaphase. The contractile ring determines a constriction forming a cleavage furrow at the cell's equatorial cortex. The constriction of the contractile ring progressively compacts the central spindle to form a thin intercellular bridge, an organelle-like structure called midbody. This transient structure undergoes a series of morphological changes during cytokinesis and contributes to cell fate determination by recruiting and organizing many proteins and factors that regulate the final separation of the two daughter cells, called abscission (Fededa and Gerlich, 2012).

### 1.1 Central spindle assembly

Cytokinesis starts during anaphase, when the MTs are stabilized and mitotic spindle organizes in a dense interdigitating and antiparallel bundles of MTs associated with multi-proteins complexes at the central region, to form the midzone (Mollinari et al., 2002). Some MTs of central spindle derive from interpolar MTs of the metaphase spindle. Central spindle assembly is mainly due to several MTs binding and bundling proteins and to regulative kinases, such as Aurora B, PLK1 (polo-like kinase 1) and CDK1 (cyclin-dependent kinase 1) (Fig. 3; Normand and King, 2010). One of the main bundling protein is PRC1 (protein required for cytokinesis 1). PRC1 acts as an homodimer that specifically binds to the interface between antiparallel MT (Zhu et al., 2006); CDK1 regulates PRC1 through its phosphorylation to avoid dimerization during anaphase. Another key factor for central spindle assembly is the tetrameric centralspindlin complex formed by two dimers of the kinesin motor protein MKLP1 (mitotic kinesin-like protein 1) and the Rho-family GTPase activating protein, MgcRacGAP (Male germ cell Rac GTPase-activating protein) (Mishima et al., 2002). Similar to PRC1, the interaction of centralspindling with MTs is inhibited by CDK1 phosphorylation before anaphase onset. During anaphase, CDK1 levels and activity strongly decrease and the centralspindlin forms higher-order clusters in a manner that is regulated by Aurora B kinase and 14-3-3 proteins. The kinase Aurora B, the scaffolding subunit inner centromere protein INCENP, Borealin and Survivin are the component of a multi-subunit complex essential of the central spindle formation, the so-called CPC (chromosome passenger complex). This complex in metaphase localizes at the centromeres, where regulates attachment of chromosomes to the mitotic spindle. After the dephosphorylation of INCENP, in anaphase, the complex localizes at the central spindle where recruits the kinesin motors MKLP1 and MKLP2. CPC not only regulates PRC1 and MKLP1, but also promotes actomyosin ring formation (D'Avino and Capalbo, 2016).

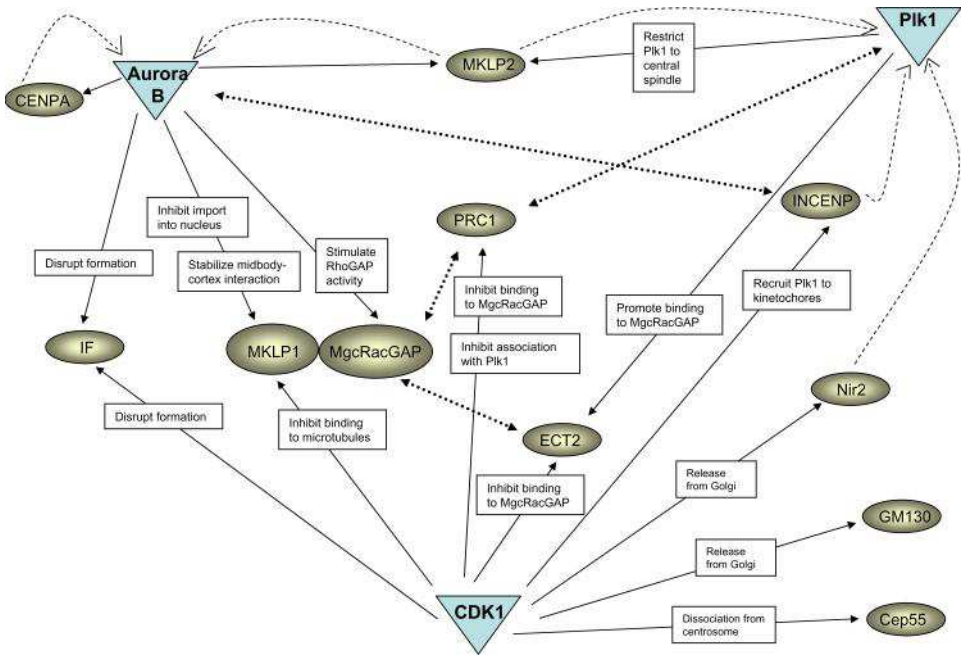


**Figure 3: Regulation of cytokinesis by mitotic kinases**
A major function of CDK1 is to prevent precocious cytokinesis before proper chromosome segregation. CDK1 thus negatively regulates some of the main players of cytokinesis. At the same time, CDK1 plays a positive role in cytokinesis by releasing cytokinesis proteins from the Golgi apparatus, and by facilitating binding of Plk1 to its substrates. Plk1 and Aurora B phosphorylate substrates that are important for both early and late steps of cytokinesis. Solid arrows indicate phosphorylation; dashed arrows indicate changed protein localization; dotted arrows indicate protein interactions. IF, intermediate filaments. (Modified by Normand and King 2010)

In this stage occurs the positioning of the division plane between the daughter nuclei; the specific site is determined through GTPase RhoA activation mediated by Rho-GEF ECT2 (epithelial cell trasforming 2) in a cascade of phosphorylations/dephosphorylations involving MgcRacGAP, PLK1 and CDK1. Another midzone motor is the kinesin-4, that accumulates at the plus end of MTs and reduces MT polymerisation and depolymerisation dynamics, stabilizing central spindle formation (Petronczi et al., 2007).

### 1.2 Cleavage furrow ingression

The pathway of RhoA, together with actin cross linking proteins, septin filaments and specific lipids, are involved in the organization and function of the actomyosin contractile ring at the cell equator. This dynamic structure, adequately RhoA-stimulated, undergoes remodeling and induces the attached plasma membrane ingression and the spacing of the separated material to the two opposite cell's poles (Severson et al., 2002).

### 1.3 Midbody formation

After the furrow ingression, the daughter cells remain connected by the midbody. At the end of the 19th century Flemming first described this dynamic organelle as tightly packed bundles of MTs with an amorphous electron dense matrix, "bulge", at its centre. Several recent studies have identified many proteins and factors, that localize at the midbody (Skop et al.2004, Hu et al.,2012). These factors are involved in several pathways, such as cytoskeletal processes, lipid rafts and vesicle trafficking. Midbody structure has been largely described, too (Hu et al., 2012). In immunofluorescence (IF) images, a non-stained region at the anti-tubulin antibodies, the so-called "dark region", is present at the center of midbody.

The organization and function of the midbody are finely regulated by the three master kinases, Cdk1, PLK1 and Aurora B (Fig. 3; Normand and King, 2010). The midbody consists of various components with dynamic distribution showing different temporal and spatial localization. According to their localization, observed by IF, the proteins of the midbody are divided into three categories: bulge, dark zone and flanking proteins. For example, as shown in the fig.4, MKLP1, MgcRacGAP and Ect2 localize at the bulge; PRC1 and KIF4A localize in the dark region; MKLP2 and Aurora B localize in the flanking zones (Hu et al., 2012).

Some components of the central spindle and contractile ring (i.e. MKLP1, KIF4, PRC1 and Aurora B) appear localize at the midbody for the whole time of their existence, and persist into a midbody remnant, a structure that, in some conditions, can persist in one of the daughter cells, after abscission. Since their asymmetric inheritance, midbody remnants are very intriguing structures, whose putative functions are still largely unknown.

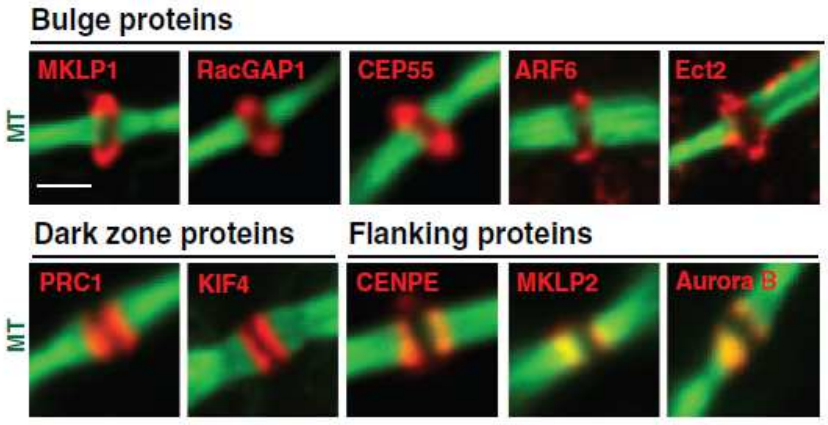


**Figure 4. Domains of midbody.**
Midbody proteins were categorized into three groups according to their localizations (Modified by Hu et al., 2012)

### 1.4 Abscission

The abscission is an actin-indipendent process that removes the cytoskeletal structure from the intercellular bridge and causes the fission of the plasma membrane, allowing the physical separation of two daughter cells. Although several recent studies were performed, the abscission's molecular mechanisms are still largely unknown.

At the intercellular bridge, when furrow ingression is complete, two symmetric sites of cortical constriction become visible and the midbody look similar to a ‘bow tie’. It was hypothesized that in this zone, some filaments forming an helix surround the midbody determines a MT rearrangement and a thinning of the midbody that indicates the scission site (Elia et al., 2012).

Several trafficking regulators, such as Spastin, SNARE (soluble N-ethylmaleimide-sensitive fusion protein attachment protein receptors), Exocysts complex components and members of ESCRTs (endosomal sorting complexes required for transport) are recruited to the abscission site just outside the flanking zone after midbody assembly as components of the abscission machinery that drive this process (Elia et al., 2011; Guizetti et al., 2011). Furthermore, trafficking vesicles are accumulated at the midbody and at the abscission site (Hu et al., 2012).

In contrast with the abundance of factors identified to localize at the midbody and at the abscission site, the mechanisms required to complete the final cytokinesis stage remains not completely understood; different models have been proposed to explain the abscission mechanism. The current model involves a complex and orderly successions of events that require many components, such as members of the ESCRT's machinery, including members of ESCRT-I, ESCRT-II and ESCRT-III. This family is involved in some events, such as the formation of multi-vesicular bodies and the maintaining the integrity of midbody. Members of this family are sequentially recruited to midbody to orchestrate membrane fission during abscission (Fig. 5; Neto and Gould, 2011). During late telophase, the ESCRT complex localizes to the midbody and its recruitment is finely regulated. As described in Fig 5, in response to complex phosphorylation events by PLK1, Cep55 (centrosomal protein 55kDa) localizes to the midbody where it is recruited by the centralspindlin component, MKLP1 (Bastos and Barr, 2010). Cep55 recruits the ESCRT-I factor Tsg101 (tumor-susceptibility gene 101) to the site of scission, together with the ESCRT-I-related protein ALIX (apoptosis-linked gene 2-interacting protein X) (Hurley and Hanson, 2010). Subsequently, multiple subunit of the downstream ESCRT-III complex CHPM4B (charged multivesicular body

protein 4B), polymerize to form spiral filaments that expose their membrane interaction sites on the surface, leading to the deformation of the MT bundles, that become progressively thinner, and transform a membrane neck into a narrow constriction (Guizetti et al., 2011). MT bundles extending from either side of the dark zone of the midbody converge in two narrow membrane-constriction site that are cleaved sequentially or only one of these sites are cleaved. Here, the member of ESCRT-III's complex CHMP1B, recruits and binds the MT severing enzyme, spastin, that cuts MTs, disassembling the intercellular bridge (Connell et al., 2009; Yang et al., 2008). A portion of the midbody including the dark zone often persists after abscission, as a midbody remnant in one of the daughter cells where it is removed by autophagy.

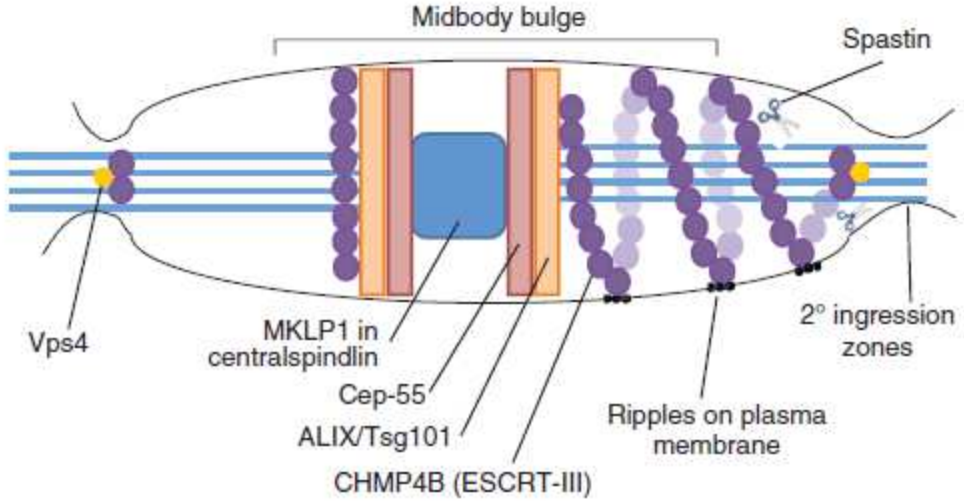


**Figure 5: The ESCRT complex in abscission.** The centralspindlin component recruits Cep-55 to the midbody. Cep-55 interacts with the ESCRT-I protein Tsg101 or the adaptor protein ALIX, which are in turn proposed to recruit ESCRT-III components. Tsg101 and the ESCRT-III subunit CHMP4B (shown here as purple spheres) are sequentially recruited into the centre of the intercellular bridge where they form a series of cortical rings, shown here in the left half of this schematic midbody (Elia et al., 2011). Later in cytokinesis, CHMP4B concentrates at the narrow secondary abscission zones, closely followed by Vps4 (yellow circles), which leads to abscission at these sites. CHMP4B forms two narrow cortical rings adjacent to the midbody prior to disassembly of the MT. ESCRT-III subunits (such as CHMP4B) extend towards these sites of cortical constriction forming a series of intertwined, regularly spaced, filaments, which extend towards the site of secondary ingression, shown here on the right of this schematic midbody. These rings also give rise to the appearance of 'ripples' on the plasma membrane. ESCRT-III can then recruit the MT-severing enzyme spastin (shown here as scissors). (Neto and Gould, 2011)

### 1.5 Spastin

Spastin is a member of the AAA (associated with a variety of cellular activities) ATPases protein family. It is encoded by the *SPG4* gene (Hazan, et al., 1999; Fonknechten et al., 2000; Lindsey et al., 2000). Mutations in the SPG4 gene occurs in 40% of autosomal dominant Hereditary spastic paraplegia (HSPs) cases, neurodegenerative disorders characterized by progressive spasticity of the lower extremities due to degeneration of corticospinal motor tracts (Soderblom and Blackstone, 2006; Blackstone, 2012). SPG4 mutations destroy the enzymatic activity of spastin leading to pathogenesis mainly by a haploinsufficiency mechanism. Alternatively, a few SPG4 cases involve dominant-negative or gain of function mechanisms.

Spastin possesses MT-severing ability and contributes to different processes involving MT/cytoskeleton, such as cytokinesis, membrane modelling, intracellular and axonal vesicle transports, number and motility MTs regulation and distribution of their dynamic plus-ends through breaking longer MTs into shorter ones (Trotta et al., 2004; Connell et al., 2009; Errico et al., 2002; Baas et al., 2006). It was observed that polyglutamylation of tubulin stimulates spastin-mediated severing most likely because of an increase in negative charge of the MT tails (Lacroix et al., 2010). Polyglutamylation and other modifications, such us acetylation, correspond to MTs stability; spastin preferentially cuts stable regions of axonal MTs compared to more labile and dynamic regions at the MTs plus-ends (Riano et al., 2009). Spastin is enriched in regions characterized by extensive MT/cytoskeleton remodelling, such as centrosome in interphase and during mitosis, midbody in cytokinesis, and growth cones and branching points in neurons (Errico et al. 2004; Yu et al. 2008).

Recently, ultra-structural studies have shown that spastin forms hexameric rings with pore loops that bind and tug the tubulin C-terminal tails to disrupt tubulin polymeric interactions and severs MTs (Fig. 6) (White et al., 2007; Roll-Mecak and McNally, 2010; Sharp and Ross, 2012).

Several evidence suggest that the precise stoichiometric levels of spastin are crucial for its biological functions and has been hypothesized that alterations in the level of spastin production contribute to the development or progression of the disease (Riano et al., 2009).

In proliferating cells, spastin is essential for ESCRT-dependent final abscission step, it is recruited by CHMP1B to the abscission site where is responsible for the final cut of the MT midbody; it catalyzes and resolves the intercellular bridge leading to the separation of

the two daughter cells. Spastin's MIT (microtubule interacting and trafficking) domain binds to CHMP1B and it is crucial to localize spastin to midbody (Fig. 7) (Reid et al., 2005).

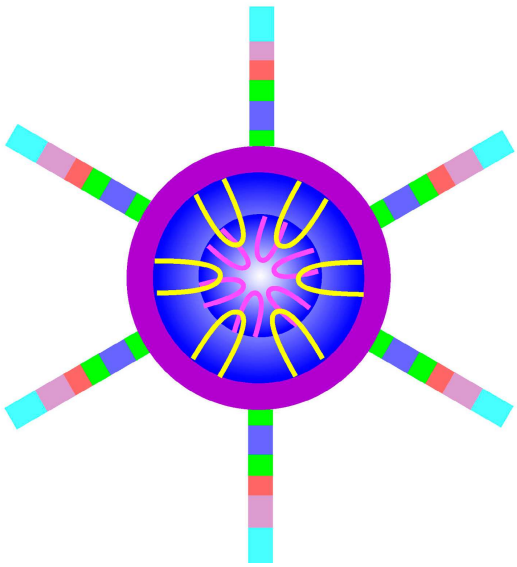

**Figure 6: Schematic depiction of domain architecture of Spastin**
Model of hexameric Spastin showing central pore and location of pore loops and N-terminal MTBD (microtubule-binding domain). The majority of the ring is formed by the AAA ATPase domain (purple). Image is looking down into the pore cavity. Each monomer of Spastin contributes two pore loops. Pore loop 1 (yellow) lies near the mouth of the pore, whereas pore loop 2 (pink) resides deeper in the pore. The N-terminal region projects from the ring. The cartoon is loosely based on structures of many AAA ATPases. (modificated by White et al., 2007)

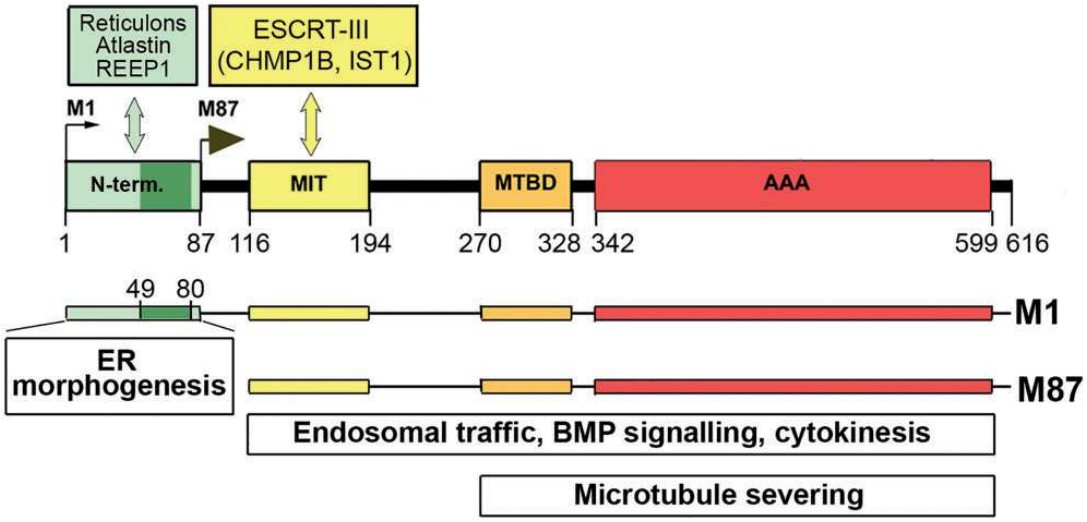


**Figure 7: Schematic representation of spastin structure**
M1 and M87 interacting proteins and involvement of spastin isoforms in cellular functions. Insertion of hydrophobic region (dark green, amino acids 49–80) of the M1-specific N-terminal domain (amino acids 1–87) into endoplasmic reticulum (ER) membrane and interaction with reticulons, atlastin and REEP1 is responsible for endoplasmic reticulum morphogenesis. Interaction of MIT domain (aminoacids 116–194) with ESCRT-III complex proteins is required for endosomal trafficking and cytokinesis. MT-binding domain (MTBD) (aminoacids 270–328) and AAA domain (aminoacids 342–599) are essential for MT severing, as well as endosomal trafficking and cytokinesis. BMP = bone morphogenic protein. (Solowska 2015)

As show in the Figure 8, spastin consists of four isoforms, generated by an additional translation initiation site and differential exon splicing: M1 full-length (616 aminoacids, 68 kDa) protein, a shorter isoform lacking the first 86 aa of the full-length protein (M87, 530 aminoacids, 60 kDa) and splice variants of both of these, excluding exon 4, (M1Δex4, 64 kDa, M87Δex4, 55 kDa) (Claudiani et al., 2005; Mancuso and Rugarli, 2008). M87 and M87Δex4 isoforms are the two major isoforms and are ubiquitously expressed, whereas M1 isoforms expression seems to be restricted to neuronal cells. M87 isoform is always more abundant than M1, in both neuronal and non-neuronal tissues. Different solubility and stability of M1 and M87 isoforms have been observed on exogenously expressed proteins suggesting that the degradation of M87 is more efficient that that of M1 (Solowska et al., 2010); however, no studies have been carried out on the endogenous spastin isoforms.

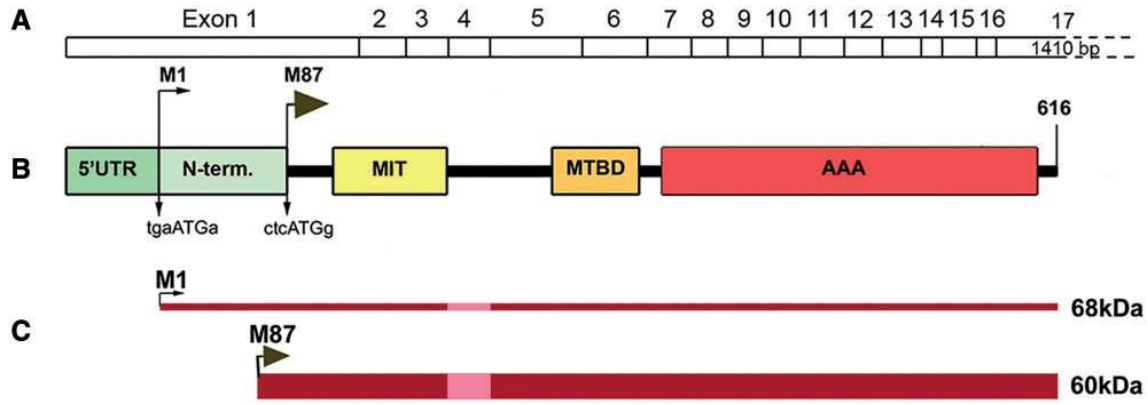


**Figure 8: Schematic representation of spastin structure.**
(A) Spastin exons 1–17. (B) Spastin functional domains: N-term = N-terminal sequence present only in M1 spastin isoform; MIT = MT interacting and trafficking domain spanning residues 116-194; MTBD = microtubule-binding domain situated between residues 270-328; AAA = ATPase associated with various cellular activities spanning residues 342-599. The Kozak's sequence tgaAUGa surrounding M1 start codon deviates considerably from a good consensus sequence g(a)ccAUGg. A better Kozak sequence ctcAUGg is present at the M87 initiation codon. (C) A leaky scanning of the first initiation codon with a poor Kozak's sequence leads to a preferred initiation of translation at the second AUG. As a result, both 68 kDa M1 and 60 kDa M87 spastin isoforms are expressed simultaneously but at different levels. A thin dark red line represents low levels of M1 expression and a dark red bar represents considerably higher levels of M87. Light red represents the M1 and M87 regions that are not present in spastin isoforms encoded by alternatively spliced mRNA lacking exon 4. (Solowska 2015)

All spastin isoforms could be recruited to the midbody, although it was reported that M87 appears to be recruited with more efficiency than M1. (Connell et al. 2009). In spastin depleted cells, the normal abscission MT breakage does not occur, daughter cells remained attached by thin, frequently very extended intercellular bridge for many hours, and this results in delayed abscission (Connell et al., 2009; Guizetti et al., 2011).

Spastin, beside to co-localize with MTs in the cell body and midbody, is present at the ER and endosomes (Reid et al., 2005; Sanderson et al., 2006). In agreement to this localization, spastin depletion leads to increased tubulation of the early endosomal compartment and to defective receptor sorting through endosomal tubular recycling compartments. An increase in complex tubular structures has also been observed in axonal growth cones of motor neurons cultured from spastin-depleted zebrafish embryos (Allison et al., 2013). Furthermore, it was demonstrated that membrane traffic and MT regulation are coupled through spastin. ATPase-defective M1 delays traffic of cargo from the endoplasmic reticulum (ER) to the Golgi network (Connell et al., 2009). Spastin is also involved in promoting axonal branching (Yu et al., 2008). Axonal branching requires delivery of new membrane to the branch site, where MT disruption is necessary and sufficient to promote delivery of membrane-bound cargoes that can insert membrane into the growing branch (Zakharenko et al., 1998). Spastin overxpression in axons results in decreased MT mass and formation of many shorter MTs due spastin's MT-severing activity (Yu et al., 2008).

At present, few studies have been carried out to investigate the mechanisms involved in the regulation of spastin expression. The transcription factors NRF1, SOX11, and ELK1 and the microRNAs (miRNAs) miR-182 and miR-96 have been involved in spastin regulation (Henson et al., 2012; Canbaz et al., 2011).

## 2. Cytokinesis defects

Progress through cytokinesis in an orderly sequence of events is crucial for the maintenance of genome stability, for the control of gene expression after cell division, and for morphogenesis and tissue homeostasis. The ability to coordinate these complex systems of trafficking and remodelling of the cytoskeleton and membranes to a precise set of temporal and indeed spatial coordinates is an essential part of the cell division; whereby it is highly regulated, mainly by reversible protein phosphorylation.

Cytokynesis failure, leading tetraploid cells, might promote genome instability and tumourigenesis. Therefore, high fidelity activity of cytokinesis' regulators is essential for the cells fate (Ganem et al., 2007; Valente et al., 2015).

Uncontrolled activation/inactivation of cytokinesis factors can lead to different defects. For example, starting cleavage furrow ingression, before the complete chromatids separation, or its precocious regression might induce midbody iperstability, the persistence of long uncut

intercellular bridge (LIBs) and binucleation. Blocking furrow ingression causes cells to accumulate with midzone-like MT assemblies (Normand and King, 2010). Errors of chromosome segregation lead to form chromosome bridge that delay abscission. In the presence of chromosome bridge, the timing of abscission is controlled by Aurora B by a regulatory pathway termed "NoCut", when Aurora B remains active and maintains MKPL1 phosphorylated (Mathieu et al., 2013). This event stabilizes the interaction between the ingression furrow and the midbody and prevents the furrow regression until chromosome bridge is disassembled (Steigemann et al., 2009). Blocking abscission factors, for example by depleting single members of ESCRT-III machineries, leads to cytokinesis failure and binucleated cell formation.

## 3. Homeodomain Interacting Protein Kinase 2 (HIPK2)

The Homeodomain Interacting Protein Kinase 2, HIPK2, is an evolutionary conserved multifunctional serine/threonine kinase, originally identified together with other two members of the HIPK family, HIPK1 and HIPK3, as interactor of homeodomain trascription factors (Fig. 9) (Kim et al., 1998).


**Figure 9.** Schematic representation of HIPK2 structural domains. N-ter: N-terminal domain; HID: Homeobox Interactive Domain; PEST: region important for HIPK2 regulation and interaction with other protein; AID: Auto-Inhibitory Domain; YH: Y and H rich domain. (Adapted from Siepi et al, 2013)

HIPK2 is involved in a lot of different signal transduction pathway and cellular events, such as cell survival, cell proliferation, transcriptional regulation, differentiation, development, apoptosis during development and DNA damage or hypoxia response, angiogenesis and antiviral responses. (Calzado et al., 2007; Rinaldo et al., 2007a; D'Orazi et al., 2012)

HIPK2 binds and phosphorylates many targets, such as trascriptional regulators, signal trasducers and chromatin modifiers (Fig. 10) (D'Orazi et al., 2002; Hofmann et al., 2002; Ritterhoff et al., 2010; Bracaglia et al., 2009). HIPK2 shows a preferential site-specific phosphorylation target at proline-flanked Ser/Thr residues. HIPK2 might act as coactivator or corepressor, depending on the promoters or the cellular context.

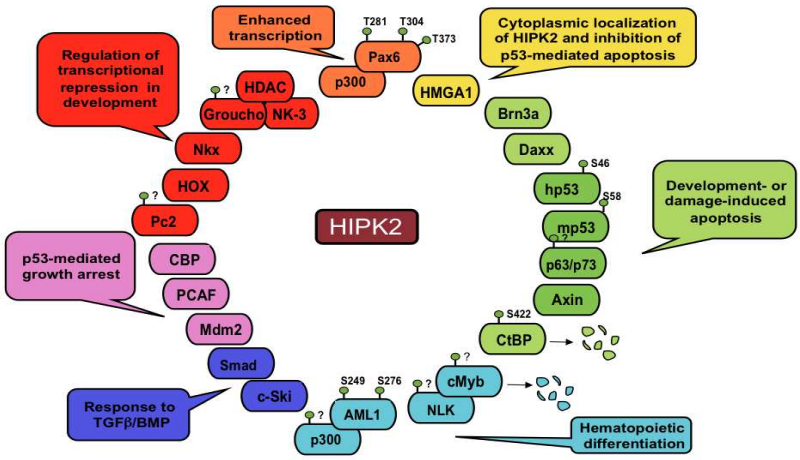


**Figure 10. HIPK2 targets.**
Schematic representation of HIPK2 targets with indicated biological activity and phosphorilation site/s (Adapted from Rinaldo et al., 2007a)

## 3.1 HIPK2 and DNA damage

The cells have generated a highly efficient signal transduction and response network to counteract and repair DNA damage.

HIPK2 plays a role in DNA damage response pathway by phosphoregulating several transcription factors and coregulators, such as the tumor suppressor p53, the p53 inhibitor MDM2, the transcriptional corepressor CtBP, the PML (tumor suppressor promyelocytic leukaemia) factor. HIPK2 and p53 colocalize at PML-Nuclear bodies and HIPK2 regulates p53 localization, phosphorylation, acetylation, and transcriptional activity. HIPK2 activity enhances both the p53-mediated trascriptional activation of proapoptotic factor, PIG3, BAX and NOXA, both the inhibition the antiapoptotic factor Galectin-3 (D'Orazi et al., 2002; Hofmann et al., 2002; Cecchinelli et al., 2006). It was demonstrated that HIPK2 is critical to control the p53 activity and to balance the cell fate of DNA damaged cells between growth arrest and apoptosis (Rinaldo et al., 2007b). In physiological conditions, HIPK2 activation is finely controlled by several protein degradation mechanisms, while in presence of DNA lesions, HIPK2 degradation is blocked. Upon DNA damage, HIPK2 binds and phosphorylates p53 at Ser46 contributing apoptosis induction and subsequent cell death (D'Orazi et al., 2002; Hofmann et al., 2002). HIPK2 can also controls DNA damage response driving degradation of the transcriptional corepressor CtBP by phosphorylation at Ser422 (Zhang et al., 2003), or controlling the activity of other apoptosis related proteins, such as p73 and p63 (Kim et al., 2002; Lazzari et al., 2011) and the p53 inhibitor MDM2 (Wang et al., 2001).

## 3.2 HIPK2, cytokinesis and genomic stability

A recent study of Rinaldo and coworkers has identified a novel role of HIPK2 in cytokinesis (Rinaldo et al., 2012). This kinase controls cytokinesis by preventing tetraploidization and genome instability (Rinaldo et al., 2012; Valente et al., 2015). In particular, it was demonstrated that HIPK2 and the extra-chromosomal histone H2B co-localize at midbody during cytokinesis. Furthermore, HIPK2 was shown to phosphorilate H2B at Ser14. The localization of HIPK2 at midbody and its H2B specific phosporilation (H2B-Ser14P) are critical for a successful cytokinesis. Indeed, HIPK2 depletion, by genetic inactivation or RNA interference or HIPK2 kinase dead mutant over-expression, results in the absence of H2B-Ser14P at midbody, causing accumulation of cytokinesis defects, such as LIBs and binucleation. Notably, the over-expression of phosphomimetic mutant H2B-Ser14D is able to rescue cytokinesis failure in Hipk2 null cells, demonstrating that a catalitically active HIPK2 is required for cytokinesis through the phosphorylation of histone H2B in Ser14 (Rinaldo et al., 2012; Figure 11).

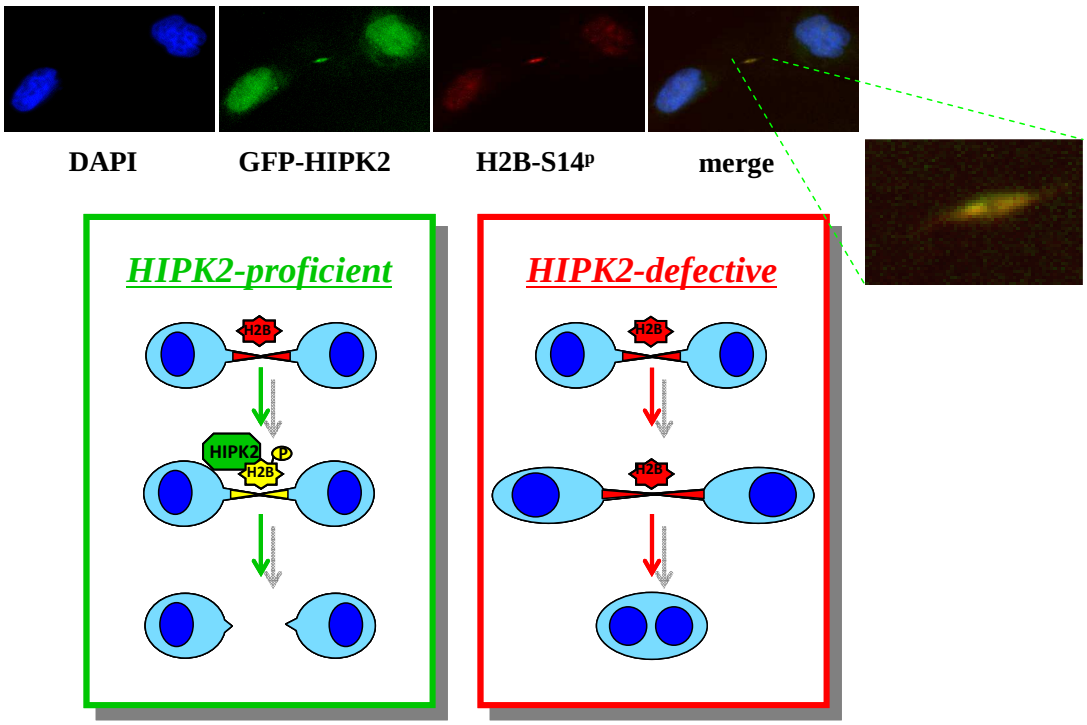


**Figure 11. Graphical representation of cytokinesis in HIPK2 proficient or defective cells**.
The IF images show HIPK2 and H2B-Ser14P localization during cytokinesis in HeLa cells. Lacks of H2B-Ser14P localization at midbody in HIPK2-defective cells results in cytokinesis defects and binucleation. (adapted from Rinaldo et al., 2012)

## 3.3 HIPK2 and cancer

HIPK2 has been reported to act as a tumour soppressor (Hofmann et al., 2012; D'Orazi et al., 2012). Reduction of HIPK2 expression leads to impaired apoptosis and induces resistance to different chemotherapeutics (Krieghoff-Henning and Hofmann, 2008; Puca et al., 2010). Hipk2-/- mice are mice more sensitive to carcinogen-induced skin cancer formation than Hipk2+/+ mice (Wei et al., 2007). Many pathways that inactive HIPK2 have been found in human cancers. In leukemogenesis and in breast carcinomas HIPK2 is trapped in cytoplasm (Wee et al., 2008; Pierantoni, personal comunications), in acute myeloid leukemia HIPK2 is mutated (Li et al., 2007), and in thyroid cancers was reported an allele-specific loss of heterozygosity (Lavra et al., 2011). A screening in thymic lymphomas demonstrated that Hipk2 is a haploinsufficient tumor suppressor gene also in vivo, with loss of one Hipk2 allele in 30% of the tumors and increased susceptibility of Hipk2+/- mice (Mao et al., 2011).

Hipk2-/- mice born at a reduced mendelian rate; though they survive and are fertile, they are smaller than their wild-type littermates throughout adulthood (Isono et al., 2006) and present proliferation defects in MEFs and in sensory neurons (Rinaldo et al., 2012 Wiggins et al., 2004). Hipk1/Hipk2 double knockout embryos die between 9.5 and 12.5 days post-coitus with proliferation defects (Isono et al., 2006). Hipk2-/- mice show an array of psychomotor abnormalities, underscoring an important role of this kinase in the nervous system (Wiggins et al, 2004; Isono et al, 2006; Zhang et al, 2007; Anzilotti et al., 2015).

Hipk2-null MEFs show cytokinesis failure and accumulate subtetraploid karyotypes developing chromosomal instability. These defects lead to inhibition of proliferation and spontaneous immortalization of primary MEFs, while increase tumorigenicity when MEFs are transformed by the E1A and Harvey-Ras oncogenes. Mice injected with E1A/Ras-transformed Hipk2-null MEFs generate tumors with genetic alterations resembling those of human cancers derived by initial tetraploidization event (Valente et al., 2015).

In conclusion, HIPK2 has many key roles in safety control of the cells, and among its oncosuppressive functions there is also the prevention of tetraploidization and genome instability.

# AIM

Cytokinesis consists of an orderly sequence of crucial dynamic events that allow the segregation of the cytoplasmic material and the physical separation of two daughter cells during cell division. Proper cytokinesis is essential for maintaining ploidy and genome stability. Its failure is known to lead to genetically unstable states, such as tetraploidization and multinucleation. These events can lead to chromosomal instability (CIN), a hallmark of human cancers, and are considered critical steps in tumor formation/progression. However, the pathways involved in this process are not yet well understood.

The oncosuppressor HIPK2 is a multifunctional serine/threonine kinase involved in different signal transduction pathways and cellular events A recent study of Rinaldo and coworkers has identified a novel role of HIPK2 in cytokinesis. This kinase regulates cytokinesis preventing tetraploidization through the phosphorylation of the extra-chromosomal histone H2B at S14. These two proteins colocalize at the midbody, the organelle-like structure formed at the cleavage furrow between the two daughter cells during cytokinesis. However, which are the cytokinesis pathways regulated by HIPK2 is still missing. HIPK2-depleted cells accumulate aberrant midbodies and fail cytokinesis, leading to CIN and increased tumorigenicity (Rinaldo et al., 2012; Valente et al., 2015).

To evaluate which cytokinesis pathways are affected by HIPK2 depletion, we first analyzed the epistatic relationships localization to the midbody of known factors of cytokinesis in HIPK2 depleted cells. Once identified factors affected by HIPK2 depletion, we characterized at the biochemical and functional levels HIPK2 cross-talk with these factors.

# RESULTS

## EPISTATIC LOCALIZATION RELATIONSHIPS ANALYZES

The oncosuppressor HIPK2 predominantly localizes to nuclear bodies in interphase, but during cytokinesis it is localized at the midbody (Rinaldo et al., 2012; Fig. 12-B). To start investigating the mechanisms underlying cytokinesis role of HIPK2 and to evaluate which cytokinesis stages are affected by HIPK2 depletion, we analyzed the epistatic localization relationships of known cytokinesis components at the midbody in HIPK2 depleted cells by immunofluorescence (IF). HIPK2 depletion (H-i) was obtained by transducting HIPK2 specific stealth siRNAs in HeLa cells. Cells transducted with siRNAs, whose sequence does not specifically recognize any human mRNA were used as control (C-i). IF was performed by using specific antibodies (Abs) previously verified and characterized. As reported in Fig. 12-A and B, we first verified the depletion of HIPK2 by Real Time RT-PCR, Western Blot (WB) and IF. We observed a drastic reduction of HIPK2 mRNA and protein levels four days after transduction. At this time no localization of HIPK2 at the midbody was detectable in H-i cells (Fig. 12-B)

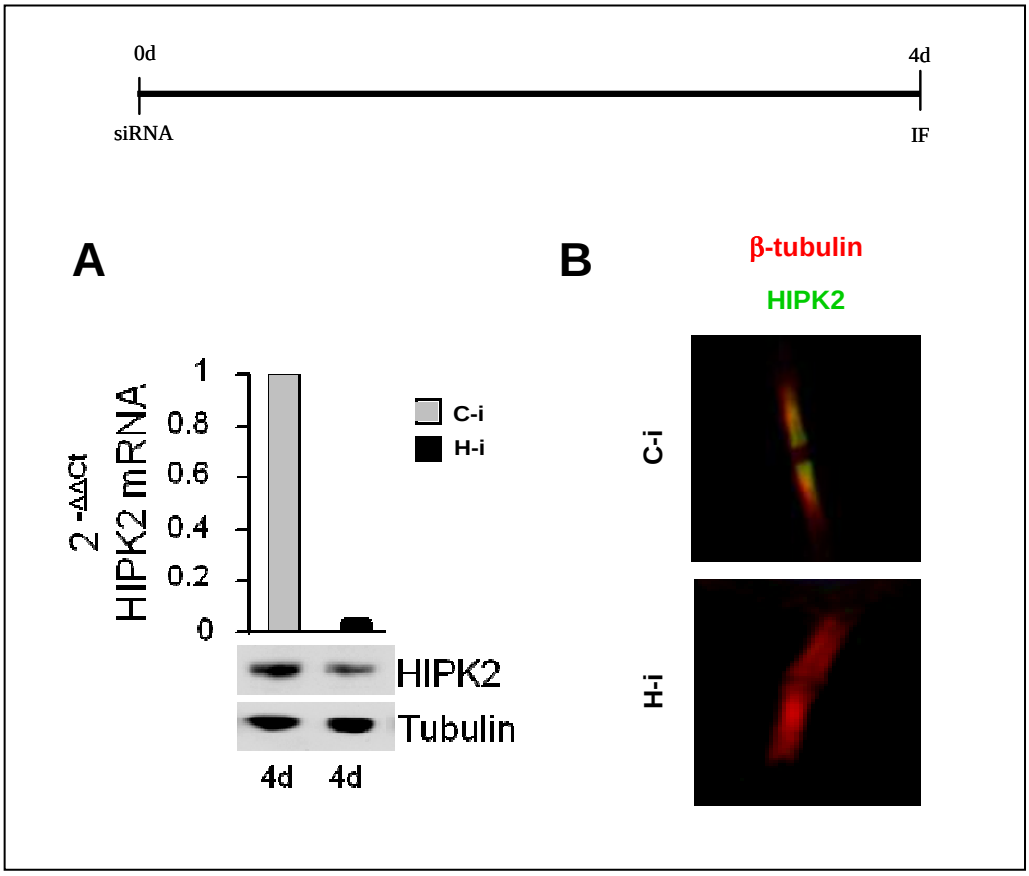


**Figure 12. HIPK2 levels post RNAi**
Upper: Schematic representation of HIPK2 interference protocol. (A) HeLa cells were transduced with control or HIPK2 siRNAs and pair samples were harvested 4 days post transduction. RNA and protein were extracted to verify HIPK2 depletion by Real-Time RT-PCR (**A**, upper panel) and by WB (**A**, lower panel), respectively. Tubulin expression was used as loading control. **(B)** Representative merged IF images of indicated cells are reported (midbody magnifications are shown). As expected, HIPK2 localizes at the flanking zone of the midbody in C-,i cells, while is absent in H-i cells. HIPK2 was marked with Ab 946 (green) and MT were marked with anti-β-tubulin Ab (red). DNA was stained with Hoechst (blue); in normal condition midbodies are negative to Hoechst-staining. d: days.

Next, we examined the spatio-temporal distribution of a series of structural and functional proteins sequentially recruited at different stages of cytokinesis at the midbody by IF. All the analyzes were performed four days after transduction.

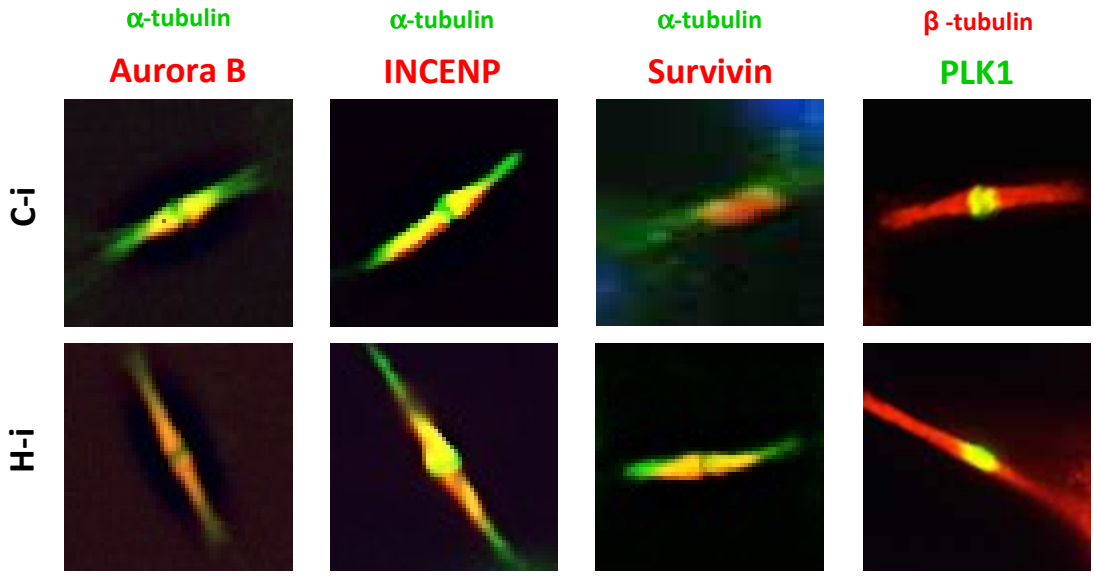


**Figure 13. HIPK2 depletion effects on the localization of master regulative kinases involved in cytokinesis.**
HeLa cells were transduced as in Fig 1. Representative merged IF images of indicated proteins in C-i and H-i cells are reported (midbody magnifications are shown). CPCs proteins (i.e. Aurora B, INCENP and Survivin) were marked with specific Abs (red); PLK1 was marked with specific Ab (green); MT were marked with anti-α-tubulin Ab (green) or with anti-β-tubulin Ab (red); DNA was marked with Hoechst (blue). N:=80 midbodies at least were analyzed for each IF.

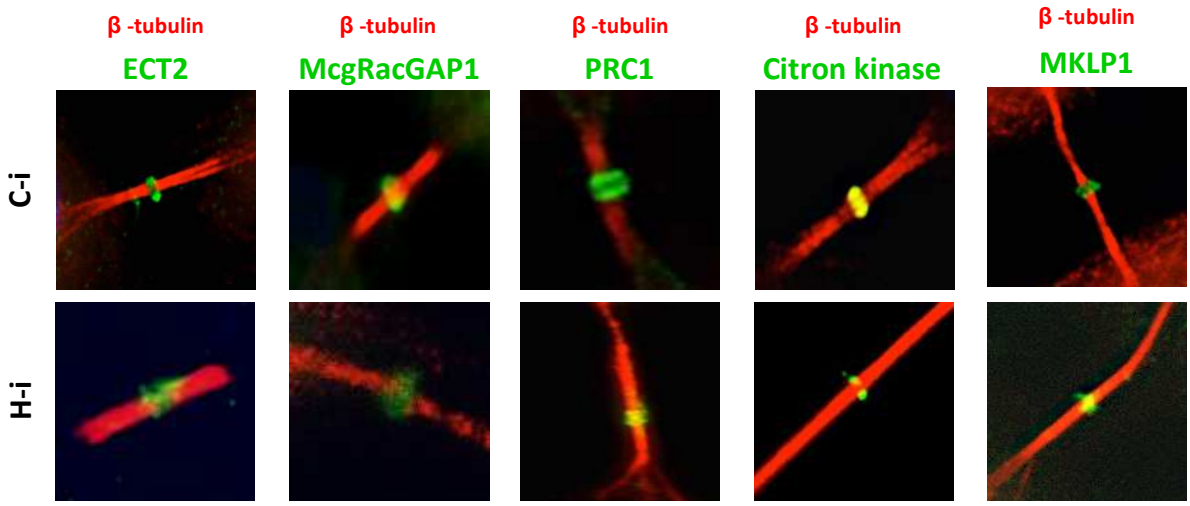


**Figure 14. HIPK2 depletion effects on the localization of proteins involved in midzone/midbody formation.**
HeLa cells were transduced as in Fig 1. Representative merged IF images of indicated proteins in C-i and H-i cells are reported (midbody magnifications are shown). Cytokinesis proteins were marked with specific Abs (green); MT were marked with anti-β-tubulin Ab (red); DNA was marked with Hoechst (blue). N=80 midbodies at least were analyzed for each IF.

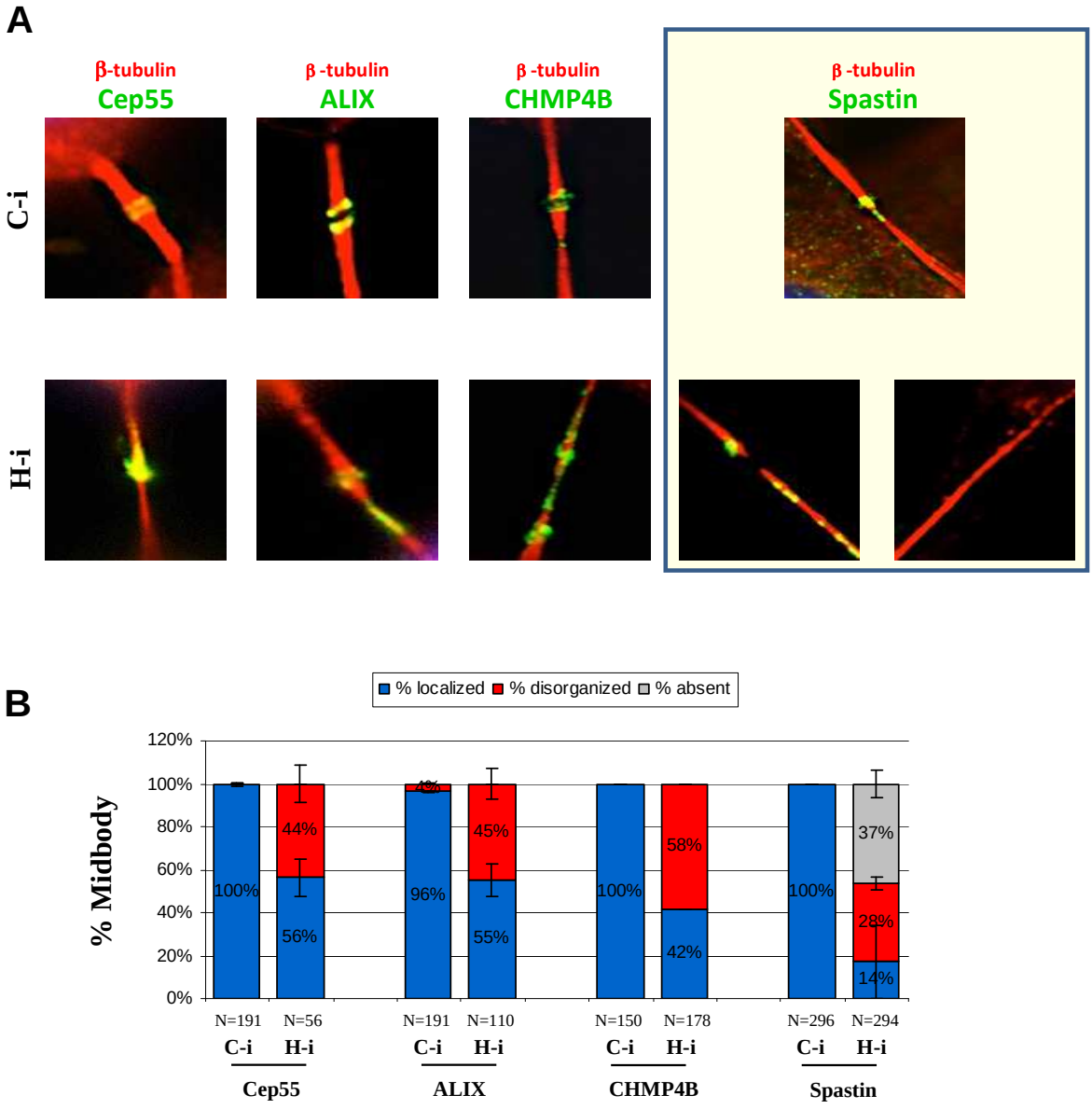


**Figure 15. HIPK2 depletion effects on the localization of proteins involved in abscission.**
(A) HeLa cells were transduced as in Fig 1. Representative merged IF images of indicated proteins in C-i and H-i cells (midbody magnifications are shown). Abscission proteins were marked with specific Abs (green); MT were marked with anti-β-tubulin Ab (red); DNA was marked with Hoechst (blue). (B) The percentage of midbodies in which the indicated proteins are localized, disorganized or absent is reported in the chart as mean±Standard Deviation (SD). N: numbers of analyzed midbodies for each IF.

As reported in the Figures 13, 14 and 15, we observed that in C-i cells all the examined proteins localize at the midbody, as expected (Hu et al., 2012). In particular: Aurora B, INCENP, survivin, PLK1 and ALIX localized at the flanking zone of the midbody; MKLP1, ECT2, MgcRacGAP1, Citron kinase and Cep55 localized at the bulge zone; PRC1 and CHMP4B localized at the dark zone; spastin localized at the flanking zone and at the site of ingression. In H-i cells, we observed that the master regulative kinases (i.e. Aurora B and PLK1) and the proteins involved in the formation/stabilization of midbody (i.e. MKLP1, MgcRacGAP1, ECT2 and Citron kinase) correctly localize at the midbody, as well as in C-i cells, indicating that midbody localization of these proteins is not affected by HIPK2 depletion. Conversely, some abscission factors, such as Cep55, ALIX, CHMP4B and spastin appear partly disorganized (i.e. they show a widespread distribution along the MT) in H-i cells, suggesting a role of HIPK2 at the abscission stage (Fig. 15-B). It is noteworthy that the MT severing spastin in the only factor which is absent at the midbody in a high percentage (37±4.9%) of H-i cells.

## HIPK2-DEPLETED CELLS SHOW ABERRANT MIDBODY RESEMBLING THOSE OF SPASTIN-DEPLETED CELLS

In HeLa cells, spastin depletion leads to delayed abscission, MT breakage does not occur, and daughter cells remained attached by LIB for many hours (Connell et al., 2009; Guizetti et al., 2011). This phenotype seems similar to that of HIPK2-depleted cells observed by Rinaldo and colleagues (Rinaldo et al., 2012). Therefore, we started to compare the midbody defects of HIPK2-depleted and spastin-depleted cells by IF. Spastin depletion was obtained by RNAi (S-i) in HeLa cells by transducting commercially available spastin-specific stealth siRNA; HIPK2 depletion was obtained as previously described; C-i cells were used as control. The depletion efficiency of both proteins was evaluated by WB (Fig. 16-A). Microscopy analyzes of fixed asynchronous cells revealed that aberrant midbodies of H-i cells are very similar to those of S-i cells. These aberrant midbodies are characterized by LIBs and MT disorganization, a phenotype that was hypothesized linked to LIBs formation and stretching condition triggered by abscission defects in S-i (Fig. 16-B; Connell et al., 2009). Furthermore, also the percentage of aberrant midbodies in H-i cells is similar to that of S-i cells (Fig. 16-C). These observations suggest a role of spastin in the cytokinesis defects of H-i cells.

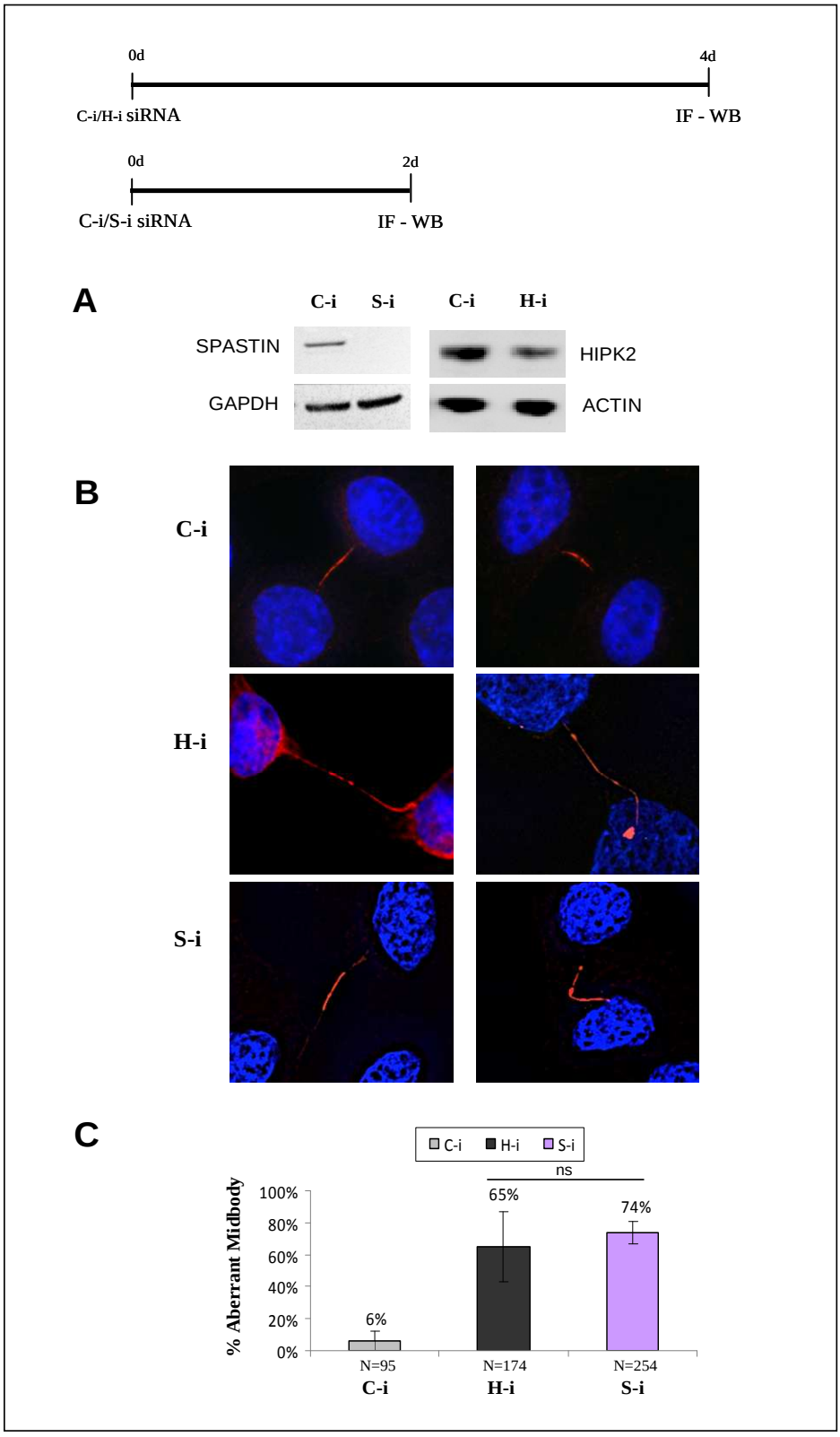


**Figure 16. Analyzes of midbody defects in HIPK2- and spastin- depleted cells**
HeLa cells were transduced with control, spastin or HIPK2 siRNAs. Schematic representation of HIPK2 and spastin interference protocols is reported (upper panel). (A) HIPK2 and spastin protein levels were analyzed by WB. GAPDH and ACTIN were used as loading control. (B) Representative merged IF images of indicated cells stained with anti β-tubulin Ab in red and DNA marked with Hoechst in blue are shown. Aberrant midbody, such as those characterized by LIBs (left panels) or MT disorganization (right panels) are showed in S-i and H-i cells. (C) The percentage of aberrant midbodies is indicated in the chart as mean±SD. ns: not statistically significant. N: number of analyzed midbodies.

## MICROTUBULES MIDBODY STABILITY IN H-i CELLS

The MT aberrant phenotype observed in H-i cells led us to hypothesize that H-i cells show a iper-stability of the MT midbody. Thus, we examined the stability of the MT midbody in H-i cells by performing a cold MT depolymerization assay in the presence of the MT depolymerising agent, Nocodazole (Fig. 17).

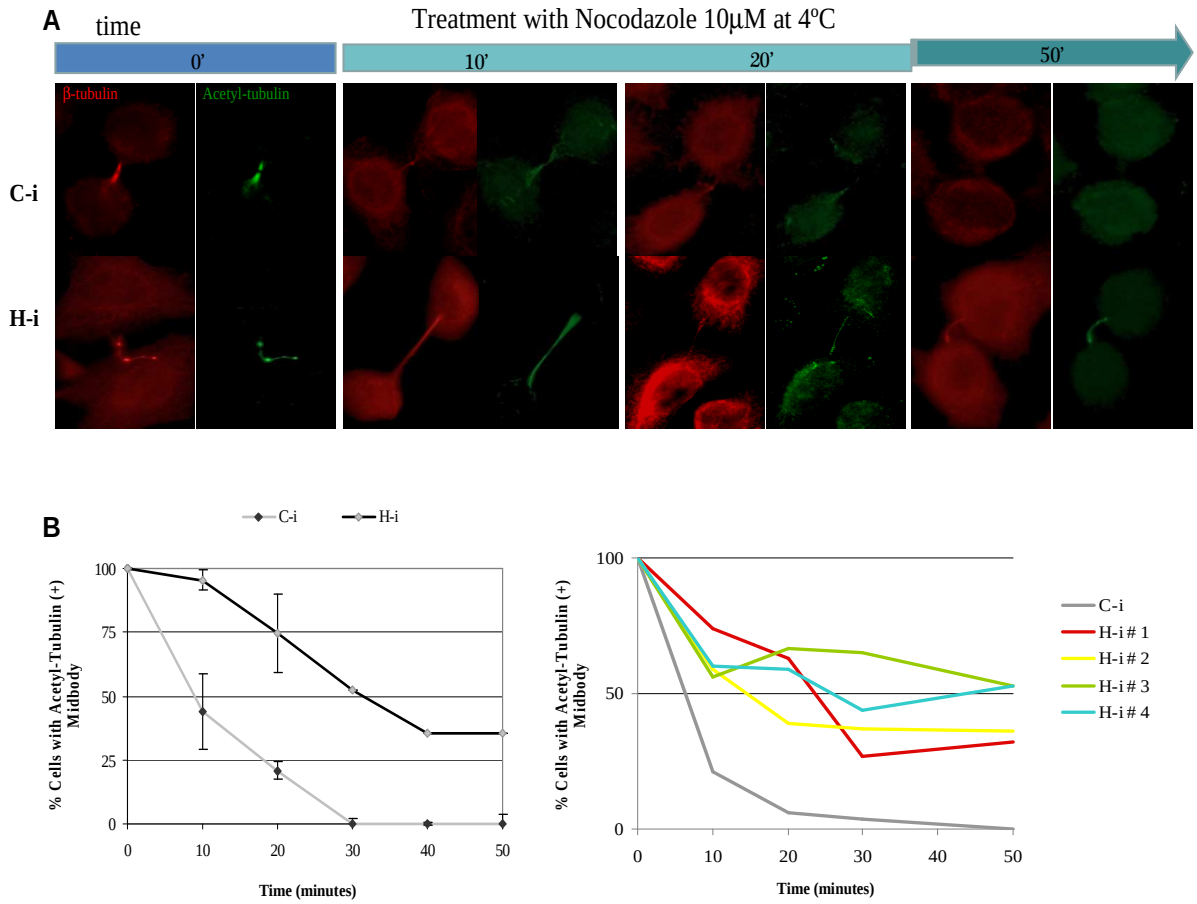


**Figure 17. MT stability assay.**
HeLa cells were transduced with control or HIPK2 siRNAs as in Fig. 12-A and treated with nocodazole at 4°C for the indicated time and then analyzed by IF 4 days post transduction. (A) Representative merged IF images of indicated cells were shown; MT were marked with anti-β-tubulin Ab (red) and acetyl-tubulin Ab (green). (B) The percentage of cells with midbodies positive for acetyl-tubulin staining is reported in the chart as mean±SD. (C) HeLa cells were transduced with control or single indicated HIPK2-specific siRNAs and treated as in A. A representative chart of the percentage of cells with midbodies positive for acetyl-tubulin staining is reported.

Cells were analyzed at different time post treatment by IF. MT midbody were marked by using not only anti-β-tubulin Ab, but also anti-Acetyl-tubulin Ab, a specific marker of stable MT (Asthana et al., 2013). As reported in the Fig. 17-A-C, we observed that Acetyl-tubulin midbody staining is completely absent 30 minutes after treatment in C-i cells. In contrast, Acetyl-tubulin midbody staining is still present in the 50% of the cells 30 minutes after treatment in H-i cells, suggesting a greater stability of the MT midbody in H-i than in C-i cells.

## EXOGENOUS SPASTIN OVER-EXPRESSION RESCUES CYTOKINESIS DEFECTS IN HIPK2-DEPLETED CELLS

Next we evaluated whether cytokinesis defects in H-i cells might be rescued by spastin exogenous expression, thus we over-expressed spastin and analyzed cytokinesis by IF in H-i cells (see Fig. 18 for protocol scheme). Flag-empty vector expressing C-i and H-i cells were used as control. Microscopy analyzes of fixed asynchronous cells show a statistically significant reduction of the percentage of binucleated cells and of aberrant midbody in transfected cells in the H-i cells over-expressing spastin variant (v) 1, compared to C-i cells over-expressing the same exogenous protein (Fig. 18-A-B). Similar data were obtained by over-expressing vectors carrying spastin v1 coding sequence fused to GFP and spastin v2 coding sequence fused to flag-myc tag (data not shown).

C-i and H-i HeLa cells were transfected with Spastin-v1 or flag-empty control vector, as above, and the abscission time (i.e., from midbody formation to abscission) was analyzed by video Time-Lapse (Fig. 19-A-C). We observed that, as expected, the abscission time is higher in flag-empty vector transfected H-i cells than in C-i cells transfected in the same manner. Notably, a significant reduction of the abscission time is evident by comparing spastin v1- and flag-empty vector- transfected H-i cells (Fig. 19-A-C), suggesting that the expression of exogenous spastin is able to partially rescue also delayed abscission phenotype in the H-i cells.

Altogether these results show that spastin over-expression is able to rescue cytokinesis defects in H-i cells.

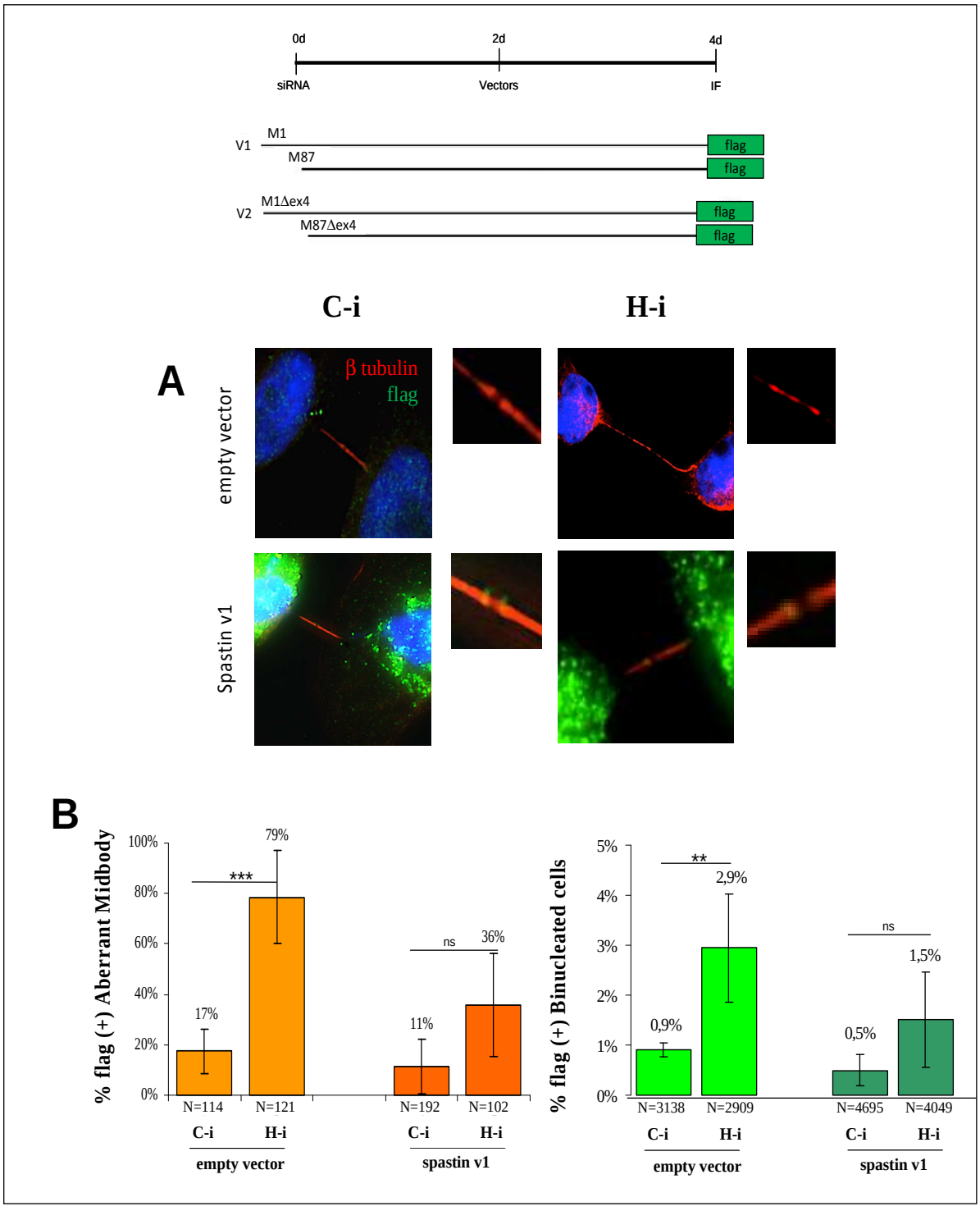


**Figure 18: Effects of exogenous spastin expression in HIPK2-depleted cells.**
Upper: Schematic representation of RNAi followed by the plasmid transfection protocol and representation of flag-myc tagged spastin isoforms expressed by each spastin variant. C-i and H-i HeLa cells were transfected with indicated vectors and analyzed by IF. (A) Representative merged IF images of indicated cells stained with anti-flag Ab in green, anti β-tubulin Ab in red, and Hoechst in blue are shown. Midbody magnification is reported at the right of each image. (B) The percentage of flag positive aberrant midbodies (left panel) and of flag positive binucleated cells (right panel) are reported in the chart as mean±SD. N: number of analyzed midbodies or cells. *** $p<0.01$; ** $p<0.05$ t test Student.

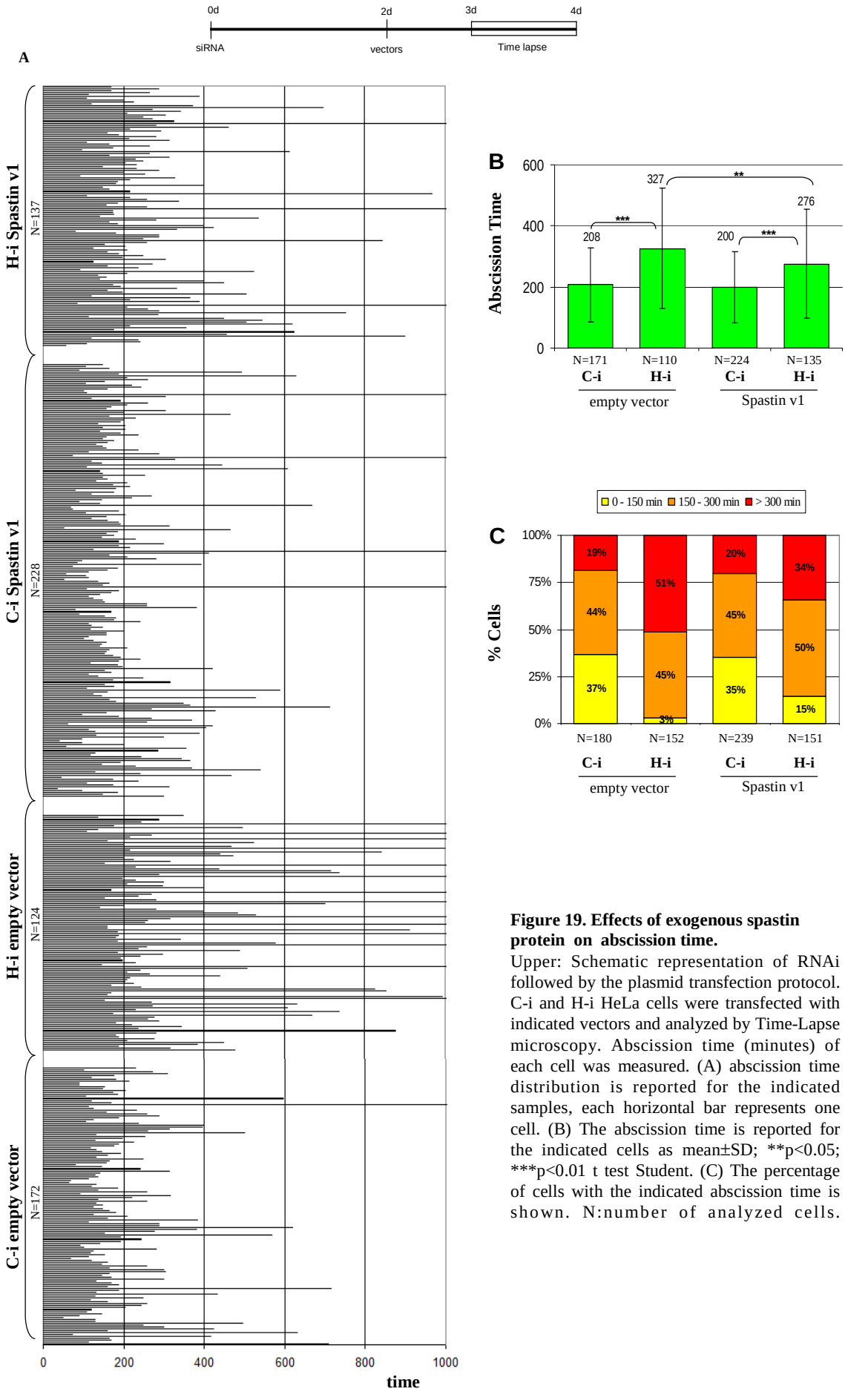


**Figure 19. Effects of exogenous spastin protein on abscission time.**
Upper: Schematic representation of RNAi followed by the plasmid transfection protocol. C-i and H-i HeLa cells were transfected with indicated vectors and analyzed by Time-Lapse microscopy. Abscission time (minutes) of each cell was measured. (A) abscission time distribution is reported for the indicated samples, each horizontal bar represents one cell. (B) The abscission time is reported for the indicated cells as mean±SD; **p<0.05; ***p<0.01 t test Student. (C) The percentage of cells with the indicated abscission time is shown. N:number of analyzed cells.

## SPASTIN OVER-EXPRESSION RESCUE CYTOKINESIS DEFECTS BUT NOT H2B PHOSPHORYLATION AT S14

It was demonstrated that a catalytically active HIPK2 is required for faithful cytokinesis through the phosphorylation of H2B at S14 at the midbody (Rinaldo et al., 2012). To analyze whether spastin over-expression rescue cytokinesis defects by acting also on H2B-S14 phosphorylation, we evaluated spastin over-expression effect on P-H2B-S14 by IF in H-i cells.

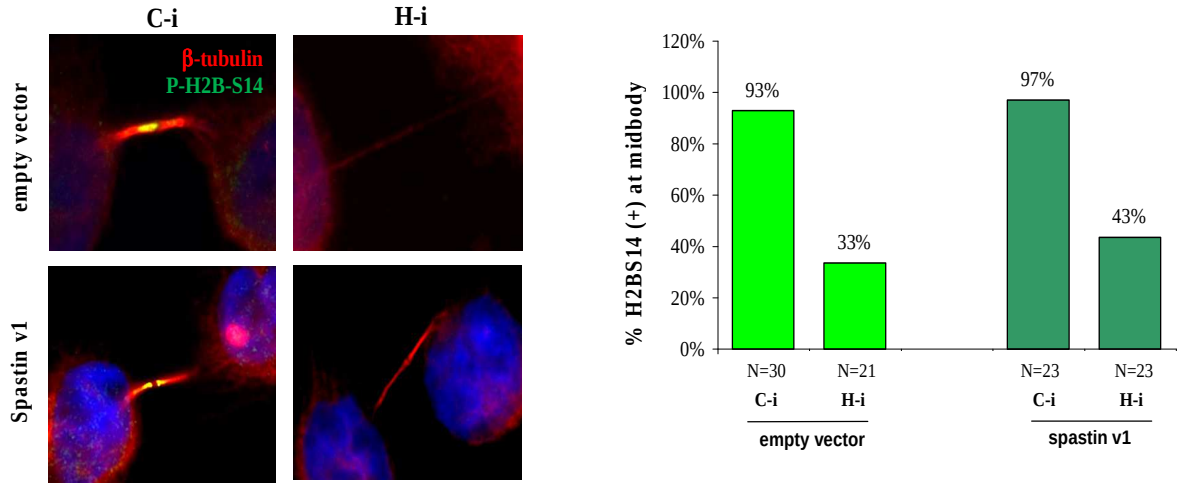


**Figure 20. Effects of exogenous spastin expression on P-H2B-S14 in HIPK2-depleted cells.**
HeLa cells were transduced with siRNA and transfected with indicated vectors as in Fig. 18, and P-H2B-S14 at the midbody localization was analyzed by IF, 4 days after transduction. Representative merged IF images of C-i and H-i cells stained with anti-P-H2B-S14 Ab in green; anti β-tubulin Ab in red and Hoechst in blue are shown (left panel). Representative chart (one of two different experiments) showing the percentage of P-H2B-S14 positive midbody in indicated cells is reported (right panel). N: number of analyzed midbodies.

We observed that the percentage of P-H2B-S14 positive midbody in H-i cells transfected with vector expressing spastin v1 (or v2; data not shown) is similar to that in H-i cells transfected with control empty vector; while, as expected, P-H2B-S14 positive midbodies are present in C-i cells transfected with empty control or vector expressing spastin v1 (Fig. 20). This result indicates that spastin over-expression rescues cytokinesis defects by acting downstream, or independently from the phosphorylation of H2B at S14.

## HIPK2 REGULATES SPASTIN

The above described results suggest the existence of a relationship between spastin and HIPK2 during cytokinesis and prompted us to investigate the mechanism underlying HIPK2/spastin crosstalk. Thus, we started to analyze the protein levels of spastin in H-i cells both in asynchronous and in telophase-enriched cells compared to C-i cells, by WB.

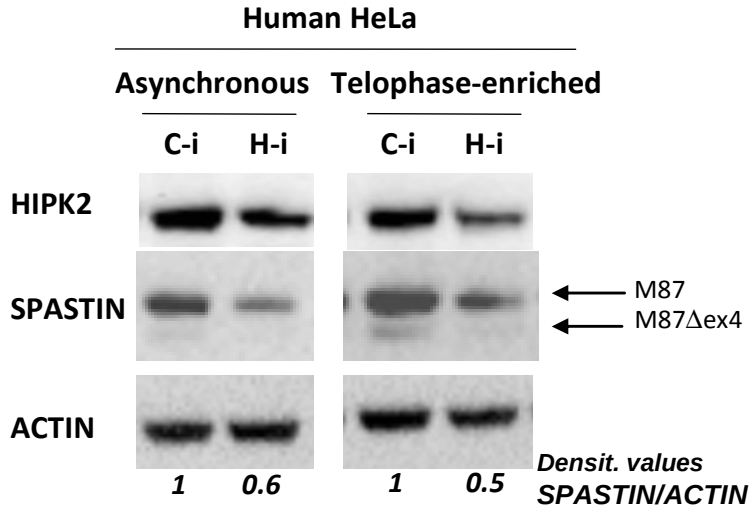


**Figure 21. Spastin levels in HIPK2-depleted cells.**
HeLa cells were transduced with HIPK2 or control siRNA as in Fig 12. Four days after transduction asynchronous cells and telophase-enriched cells were analyzed by WB. ACTIN expression was used as loading control. Densitometric analyzes were performed. As already reported (Connell et al., 2009) and as expected for non-neuronal cells, only the two isoforms of spastin, M87 and M87Δex4, are expressed in HeLa cells.

We observed a decrease of both detectable endogenous spastin isoforms in H-i compared to C-i cells. This reduction is observed in a mixed population of asynchronous cells as well as in telophase-enriched cells, suggesting that it is not a telophase-specific event (Fig. 21).

To exclude cell-specific events we verified that spastin decrease occurs in several different cell lines other than HeLa, such as in human lung adenocarinoma H1299, murine embryonal carcinoma p19 and murine immortalized motoneurons NSC-34. In all these cells protein levels of spastin decrease after HIPK2 depletion (Fig. 22).

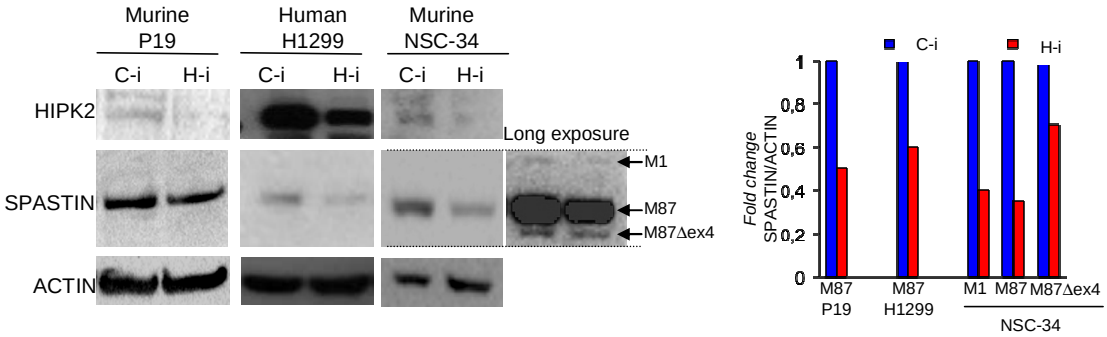


**Figure 22. Spastin protein levels in different HIPK2-depleted cells**
Indicated cells were transduced with control or HIPK2 siRNAs as in Fig 12A. HIPK2 and Spastin protein levels were analyzed by WB, four days post transduction. Representative WB showing a drastic reduction of endogenous spastin protein levels in H-i cells are reported on the left. Right image show the fold changes in the densitometric values of indicated spastin isoforms (normalized against ACTIN). To be note, as expected, M1 spastin isoform is present only in the neuronal cells NSC-34. M1Δex4 is less expressed than M1 in NSC34 cells and is not clearly detectable in this WB condition.

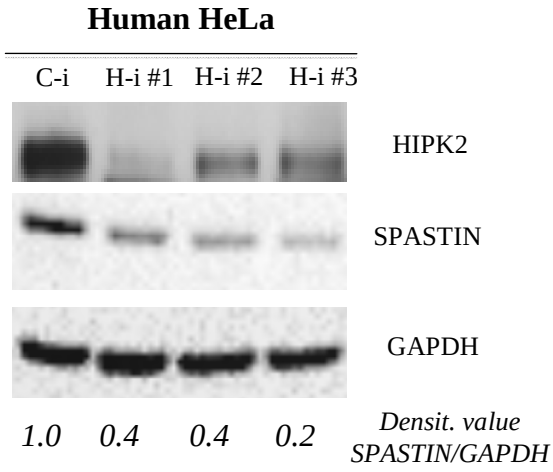


**Figure 23. Spastin protein levels after single HIPK2 siRNA transduction**
HeLa cells were transducted with indicated single HIPK2 siRNA. HIPK2 and Spastin protein levels were analyzed by WB four days post transductions. Densitometric analyses were performed.

To exclude RNA interference off-target effects, we verified that spastin reduction occurs also by transducing each HIPK2-specific siRNA alone (Fig. 23).

Furthermore, we observed that the over-expression of exogenous HIPK2 leads to an increase of endogenous spastin levels (Fig. 24).

Altogether, these findings show that HIPK2 regulates spastin expression.

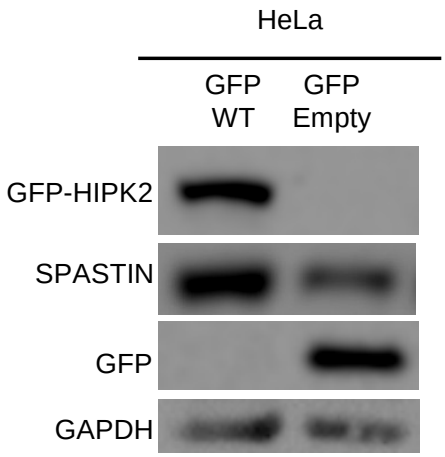


**Figure 24. HIPK2 over-expression increases endogenous spastin protein levels.**
HeLa cells were transfected with indicated GFP-HIPK2 wt or GFP expressing vectors and protein levels of indicated proteins were analyzed by WB 24 hours post transfection.

## HIPK2 REGULATES SPASTIN IN A POST-TRANSCRIPTIONAL MANNER

Next, to understand the mechanism underlying HIPK2-dependent spastin regulation, we analyzed at which level HIPK2 regulates spastin. Because HIPK2 was demonstrated to act as a transcriptional co-regulator of several promoters (Rinaldo et al., 2007; D'Orazi et al., 2012), we compared RNA and protein levels of spastin by Real Time RT-PCR and WB in H-i cells. We observed that HIPK2 depletion does not significantly affect spastin mRNA levels, suggesting that HIPK2 regulates spastin at post-transcriptional level (Fig. 25).

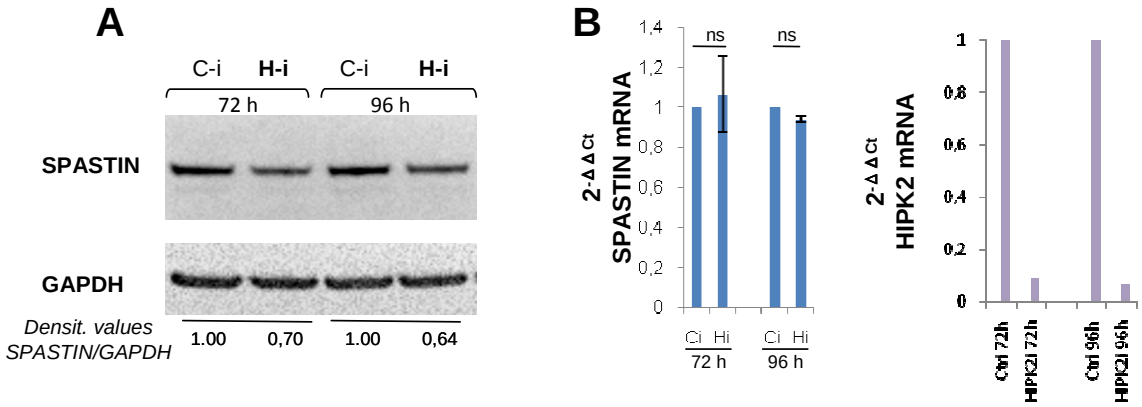


**Figure 25. HIPK2 interference down-regulates Spastin in a post-transcriptional manner.**
A-B, HeLa cells were transduced with control or HIPK2 siRNAs as in Fig. 12-A, pair samples were collected and used to analyze protein and mRNA levels of HIPK2 and spastin by WB (A) and by Real Time RT-PCR (B), respectively at indicated time post transduction. GAPDH expression was used as loading control. Densitometric analyzes were performed.

In agreement with this result, we observed that there is a negative regulation of its expression also when spastin is expressed under the control of an exogenous promoter in H-i cells. In particularly we analyzed the effects of HIPK2 depletion on exogenous spastin variants. Two days post siRNA transduction, we transfected H-i and C-i cells with plasmids expressing one the two spastin variants (i.e. Spastin-v1-flag-myc-tagged and Spastin-v2-flag-myc-tagged) under the control of a CMV promoter. Flag empty vector was used as control. Cells were collected and analyzed by WB two days post plasmid transfection. As show in the Fig. 26, a strong reduction of endogenous and exogenous spastin isoforms was observed in H-i compared to C-i cells. Similar data were obtained also by trasfecting vectors expressing spastin variant 1 fused to GFP (data not shown). These findings indicate that HIPK2 regulates spastin at post transcriptional level and that HIPK2 might control the expression of all the known spastin isoforms.

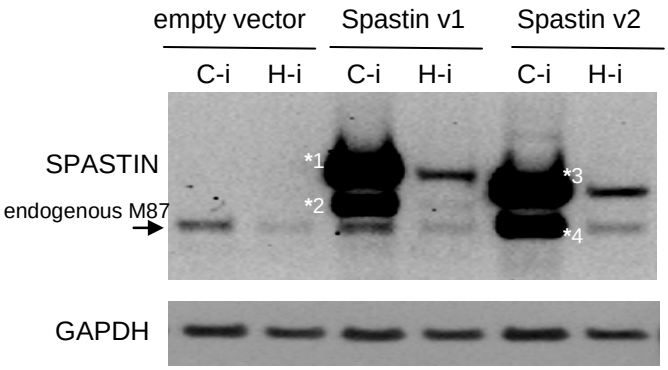


**Figure 26. Effects of HIPK2 depletion on exogenous spastin proteins.**
HeLa cells were transduced with control or HIPK2 siRNAs, transfected with indicated plasmids and analyzed by WB two days after siRNAs transduction. Representative WB is shown for indicated proteins. *1=M1, *2=M87, *3=M1Δexon4, *4=M87Δexon4 are exogenous tagged proteins. WB analyzes was also performed by using anti-flag and anti-myc Abs to further confirm the down-regulation of exogenous spastin isoforms (data not shown). As already reported (Solowska et al., 2014), when start codons of both isoforms had equally good Kozak's sequences allowing equally efficient translation, as in our spastin expressing vectors, M1 isoforms accumulate significantly more than corresponding M87.

## HIPK2 REGULATES SPASTIN IN A PROTEASOME-DEPENDENT MANNER

To get an early indication of possible pathways involved in post-transcriptional regulation of spastin mediated by HIPK2, we used different inhibitors, such as the proteasome inhibitor, MG132, and the pan-caspase inhibitor, Zvad-fmk. Cells were treated four days post

interference and analyzed by WB. The solvent dimethylsulfoxide (DMSO) was used as control.

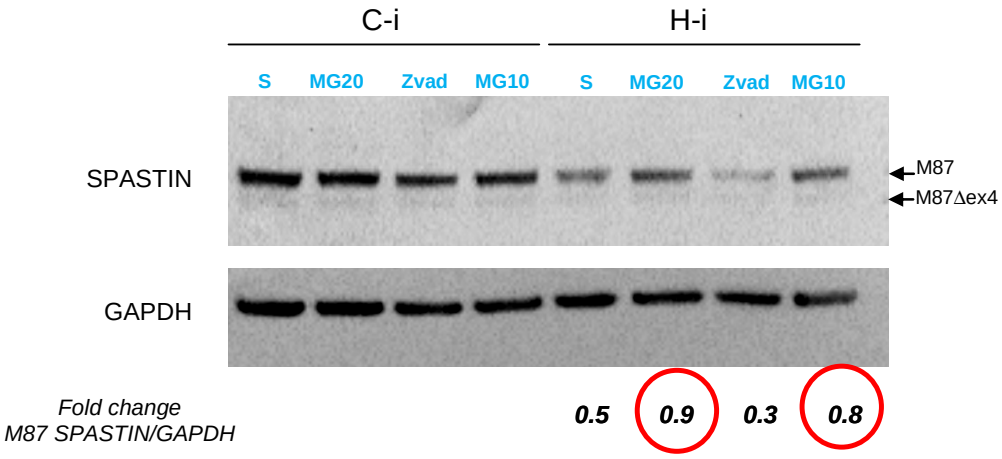


**Figure 27: Spastin down-regulation in H-i cells is proteasome-dependent**.
HeLa cells were transduced with control or HIPK2 siRNAs as in Fig. 12-A and treated with indicated inhibitors or their solvent (S) DMSO. Four days post transduction cells were collected, 8 hours post inhibitor treatment, and analyzed by WB for indicated proteins. Densitometric analyzes was performed and for each treatment fold change were calculated, as ratio of spastin levels, normalized with GAPDH, between H-i samples and relative C-i. MG10=MG132 10μM; MG20=MG132 20μM; ZVAD=pan Caspase inhibitor ZVAD-fmk 50μM.

We observed that caspases inhibition does not rescue spastin protein levels in H-i cells, suggesting that caspases pathway are not involved in HIPK2-mediated spastin regulation. In contrast, proteasome inhibition partially rescues endogenous spastin protein levels in H-i cells, indicating that spastin is regulated in a proteasome-dependent manner in HIPK2-depleted cells.

## HIPK2 REGULATES SPASTIN IN A PHOSPHORYLATION-DEPENDENT MANNER

Since HIPK2 is a kinase that regulates the stability of many of its substrates through phosphorylation, we investigated whether HIPK2 kinase activity is necessary to regulate spastin protein levels. Thus, we over-expressed HIPK2 wild-type (wt) or HIPK2 kinase dead mutant, K221A, and analyzed the effects on spastin protein levels by WB. As show in Fig. 28, the over-expression of HIPK2 wt, but not kinase-dead mutant, leads to an increase of endogenous spastin protein levels, indicating that HIPK2 kinase activity is required for spastin regulation.

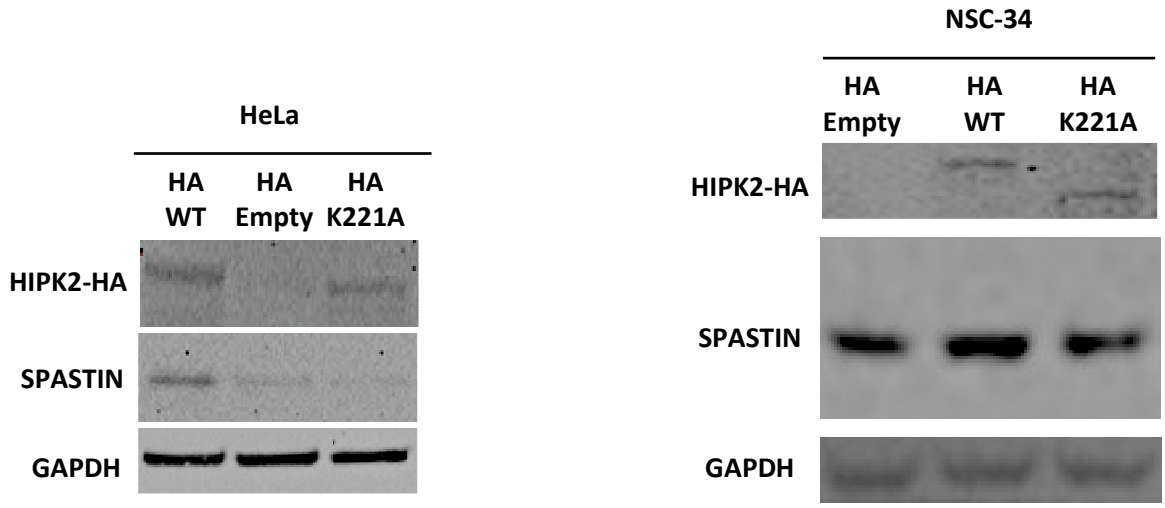


**Figure 28. HIPK2 over-expression regulates endogenous spastin protein levels.**
HeLa and NSC-34 cells were transfected with indicated expressing vectors. Protein levels of exogenous HIPK2 and endogenous spastin were analyzed by WB 24 hours post transfection. As expected, K221A band migrates slower than wt, since K221A mutant is not able to auto-phosphorylate.

## HIPK2 BINDS AND PHOSPHORYLATES SPASTIN IN VITRO

Next, we asked if spastin is target of HIPK2 phosphorylation. Thus, we evaluated the capability of HIPK2 to phosphorylate spastin in vitro. We performed in vitro kinase assay as described in Rinaldo et al., 2012, by using the four spastin isoforms as substrates and HIPK2 kinase domain as enzymatic source. We found that HIPK2 phoshorylates all the four known spastin isoforms (Fig. 29-A). Furthermore, we observed that HIPK2 is able to phosphorylate also an internal fragment of spastin variant 2 containing aminoacids from 79 to 278 (Spastin-v2 79-278; Fig. 29-B).

Next, in collaboration with Dr. Serena Camerini and Dr. Marco Crescenzi at the Istituto Superiore di Sanità (ISS), we performed tandem mass spectrometry (MS) analyzes on cold kinase assay performed by using spastin-v2 79-278 as substrate. We found a phosphorylation on spastin at Serine 268 (Fig. 30), a residue preceded by a proline (AP**S**YS), a consensus motif already reported for other HIPK2 targets (Cecchinelli et al., 2006). Interestingly, S268 is an evolutionary conserved residue common to all the four spastin isoforms and is reported phosphorylated also in several large-scale proteomic MS analyzes performed in human, as well as in murine cells (http://www.phosphosite.org/proteinAction.do?id=8325).

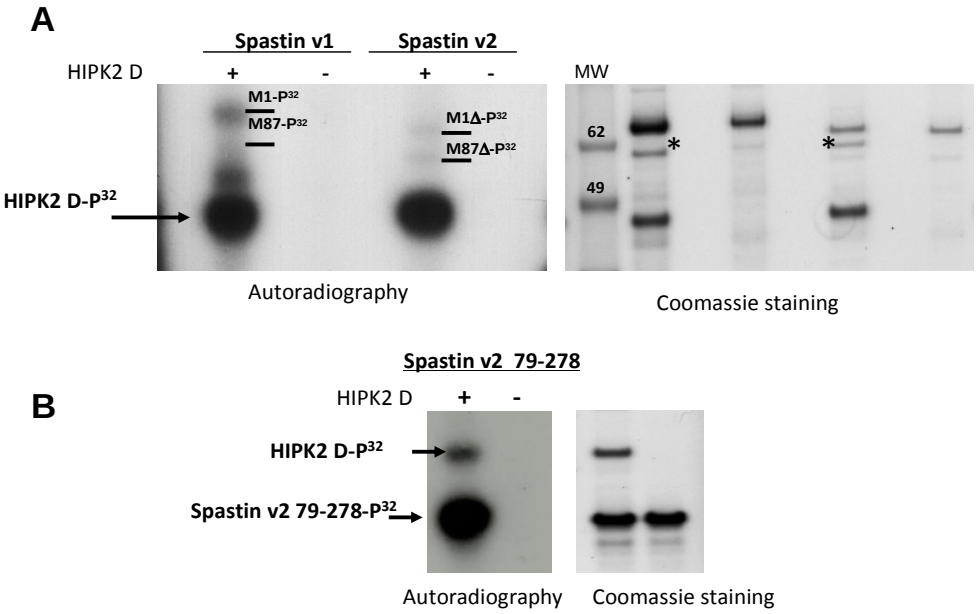


**Figure 29. Spastin is phosphorylated by HIPK2 in vitro.**
In vitro kinase assay was performed by using γATP-$P^{32}$ and HIPK2 kinase domain enzymatic source on indicate substrates. Spastin variant 1 and variant 2 flag-myc-tagged proteins were purchased by OriGene. Spastin variant 2 79-278 aa-His-tagged fusion protein was purchased by Proteintech. MW: Molecular Weight. *=chaperone protein present in our HIPK2 kinase domain preparation (kind gift from Dr.Savino).

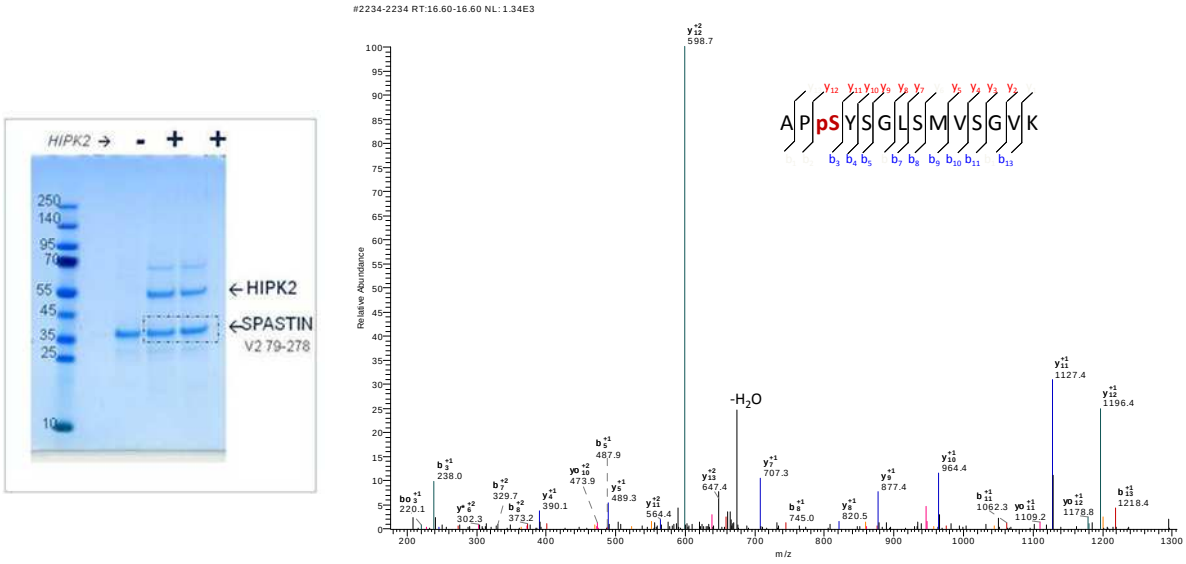


**Figure 30. Mass Spectrometry**
(A) Gel electrophoresis of cold kinase assay products; indicated bands were cut and processed in gel via tryptic proteolysis. Each peptide mixture was analyzed by MALDI-ToF mass spectrometer. (B) MS3 spectrum derived from the fragmentation of the phosphorylated spastin peptide (266-289). MS3 spectrum obtained by the fragmentation of the double charged ion 682.98. This ion has been produced by 49 Da neutral loss in the previous MS2 collision-induced dissociation of the precursor ion 731.85 (*m/z* = 731.85 → 682.98). m/z 731.85 corresponds to the double charged spastin peptide (266-289) carrying 80Da mass increment. In the MS2 scan, this ion looses a phosphoric acid molecule (-49Da) giving rise to the daughter ion with m/z 682.98. The sequence of spastin peptide (266-289) is reported in the inner panel: b and y series ions detected in the MS3 spectrum are indicated in blue and red, respectively. The presence of the almost complete y-series (from y2 to y11) without any mass increase and the occurrence of the y11 and the b-series (from b3 to b13) carrying the mass decrease due to the neutral loss confirm the localization of the phosphorylation on the serine 268.

In addition, we investigated whether HIPK2 is able to directly bind Spastin-v2 79-278 in vitro. As shown in the Fig. 31, we observed a slight specific biding between spastin internal fragment and GST-HIPK2 compared to GST alone, at least when the binding assay was performed at higher saline concentration. Consistently, we found that exogenous spastin protein (i.e. Spastin-v1-flag-myc-tagged protein) is able to co-immunoprecipitate exogenous HIPK2 (i.e. GFP-HIPK2) when over-expressed in HeLa cells (Fig. 31), suggesting that HIPK2 and spastin might physically interact.

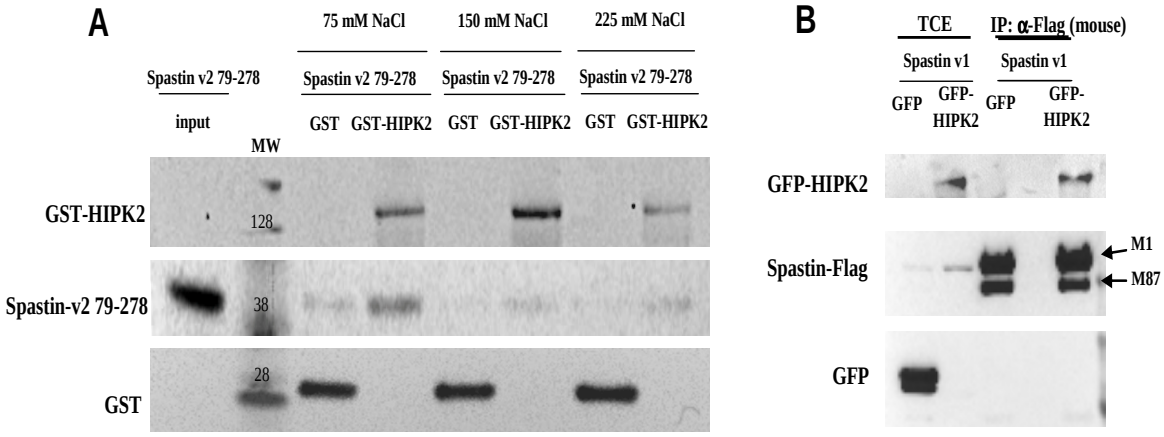


**Figure 31: HIPK2is able to bind spastin.**
(A) Binding in vitro with indicated proteins. GST and GST-HIPK2 proteins were purified from Hek293 transfected cells (see Materials and Methods for details) and incubated with 100ng of Spastin-v2 79-278-his-tagged protein (purchased by Proteintech). Input=50ng Spastin-v2 79-278. (B) HeLa cells were transfected with indicated vectors and TCEs were obtained 24 hours post transfection. IP with anti-flag monoclonal Ab (anti-DDK by OriGene) was performed. WB for indicated proteins is shown. MW: Molecular Weight.

## S268 PHOSPHORYLATION SITE IS CRUCIAL FOR SPASTIN PROTEIN LEVELS

Taking together all our data, we investigated the possibility that the regulation of spastin mediated by HIPK2 occurs through phosphorylation at S268. Thus, we generated by site-directed mutagenesis a spastin mutant that mimic a constitutive phosphorylation (i.e. S268D) and a spastin mutant that cannot be phosphorylated (i.e. S268A). These mutants were genereted in the spastin v1 context, since the isoforms expressed from this variant (i.e. M1 and M87) are those commonly more abundant in all cell types; while isoforms expressed by v2 (i.e. M1Δex4 and M87Δex4) are present at very low levels in the cells (Solowska et al., 2010). Next, we evaluated the protein levels of these mutants when expressed with a similar

transfection efficiency in HeLa cells. We observed that at different time-points after transfection and reproducibly in different sets of experiments, S268A spastin mutant isoforms show lower protein levels than wt and mutant S268D isoforms, suggesting a lower stability of the non-phosphorylable mutant and that the phosphorylation at S268 might be crucial for spastin protein levels.

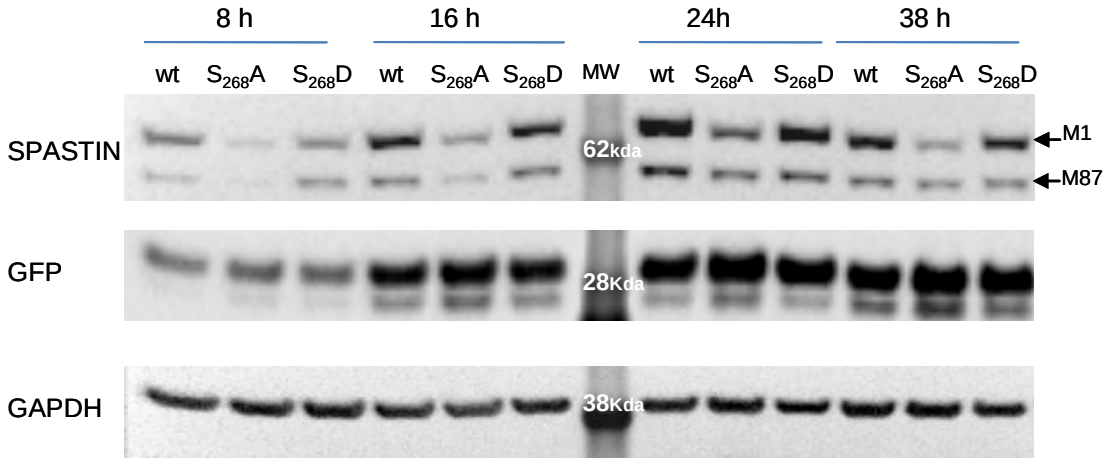


**Figure 32. Protein levels of spastin mutants.**
HeLa cells were transfected in combination with plasmids expressing spastin-v1 wt, S268A or S268D flag-myc-tagged isoforms and GFP-empty vector. Exogenous spastin protein levels were analyzed by using anti-flag Ab by WB at indicated time; GFP expression was used as an internal control for transfection efficiency. As above described, plasmids carrying Spastin-v1-flag-myc-tagged wt and mutated isoforms express both M1 and M87 isoforms. MW: Molecular Weight. h: hours.

Before using these mutants in functional studies, although S268 is outside spastin ATPase and MTBD domains (Fig. 7), we decided to verify that S268 mutations do not affect spastin severing activity on MT. Thus, we analyzed the effects of the over-expression of spastin mutants on cytoskeleton MT by IF. Spastin wt over-expression was used as control. As reported in literature (Errico et al., 2002), we observed that cytoskeleton MT appear less intense in the wt spastin transfected cells compared to untransfected cells (Fig. 33, upper panels). This effect, indicative of MT disassembly is evident also in spastin S268A and S268D transfected cells (Fig. 33, middle and lower panels), suggesting that S268 mutation sdoes not affect spastin activity on MT.

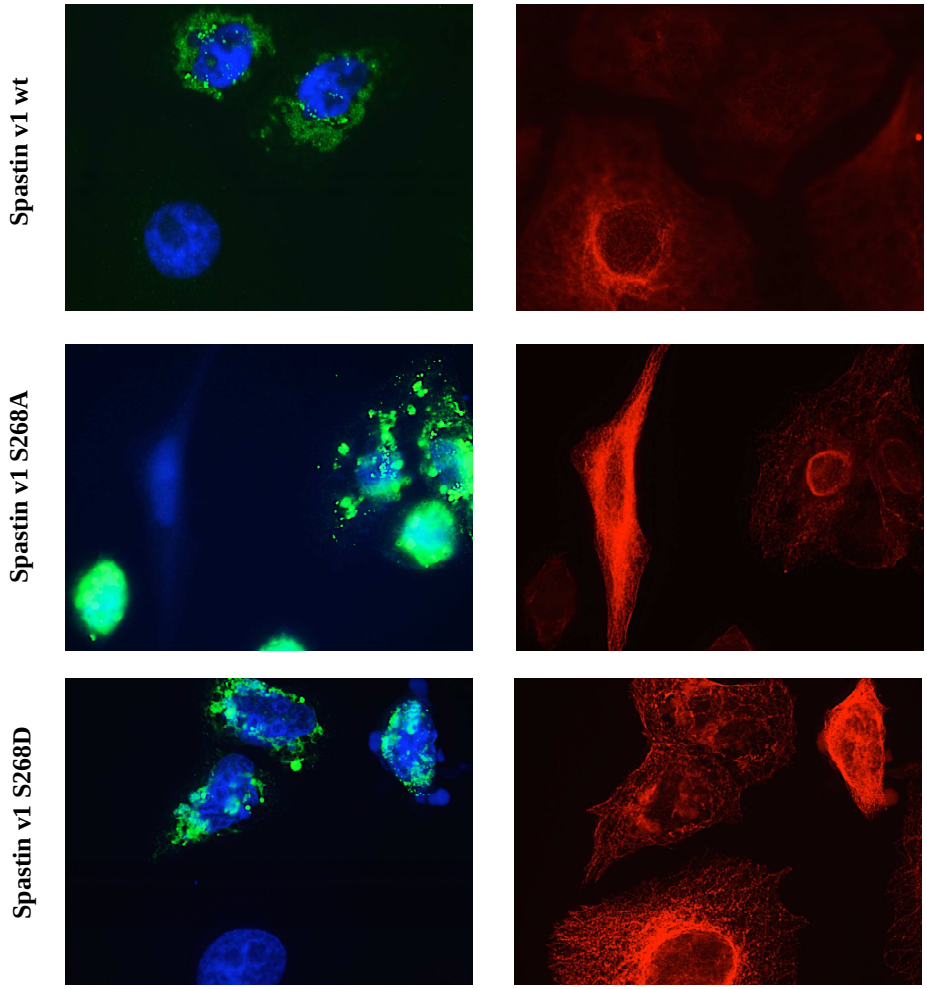


**Figure 33. Effects of spastin mutant over-expression on cytoskeleton MT.**
HeLa cells were transfected with indicated vectors and analyzed by IF 48 hours post transfection. Representative IF imagines of cells stained with anti-flag Ab in green and Hoechst in blue (left panels) and with anti β-tubulin Ab in red (right panels).

## SPASTIN S268A MUTANT OVER-EXPRESSION DOES NOT RESCUE CYTOKINESIS DEFECTS IN H-i CELLS

Since we demonstrated that spastin wt over-expression rescues the cytokinesis defects in H-i cells (Fig. 18), we analyzed the effects of S268 mutants over-expression on cytokinesis in H-i cells by IF. We observed that spastin S268D mutant, but not S268A mutant, over-expression strongly reduce MT aberrant phenotype, as well as spastin wt over-expression, in H-i cells (Fig. 34 A-B). Accordingly, by counting the percentage of binucleation in transfected cells, we found that only the over-expression of spastin S268D mutant, but not S268A mutant, rescues cytokinesis failure, as well as spastin wt over-expression, in H-i cells.

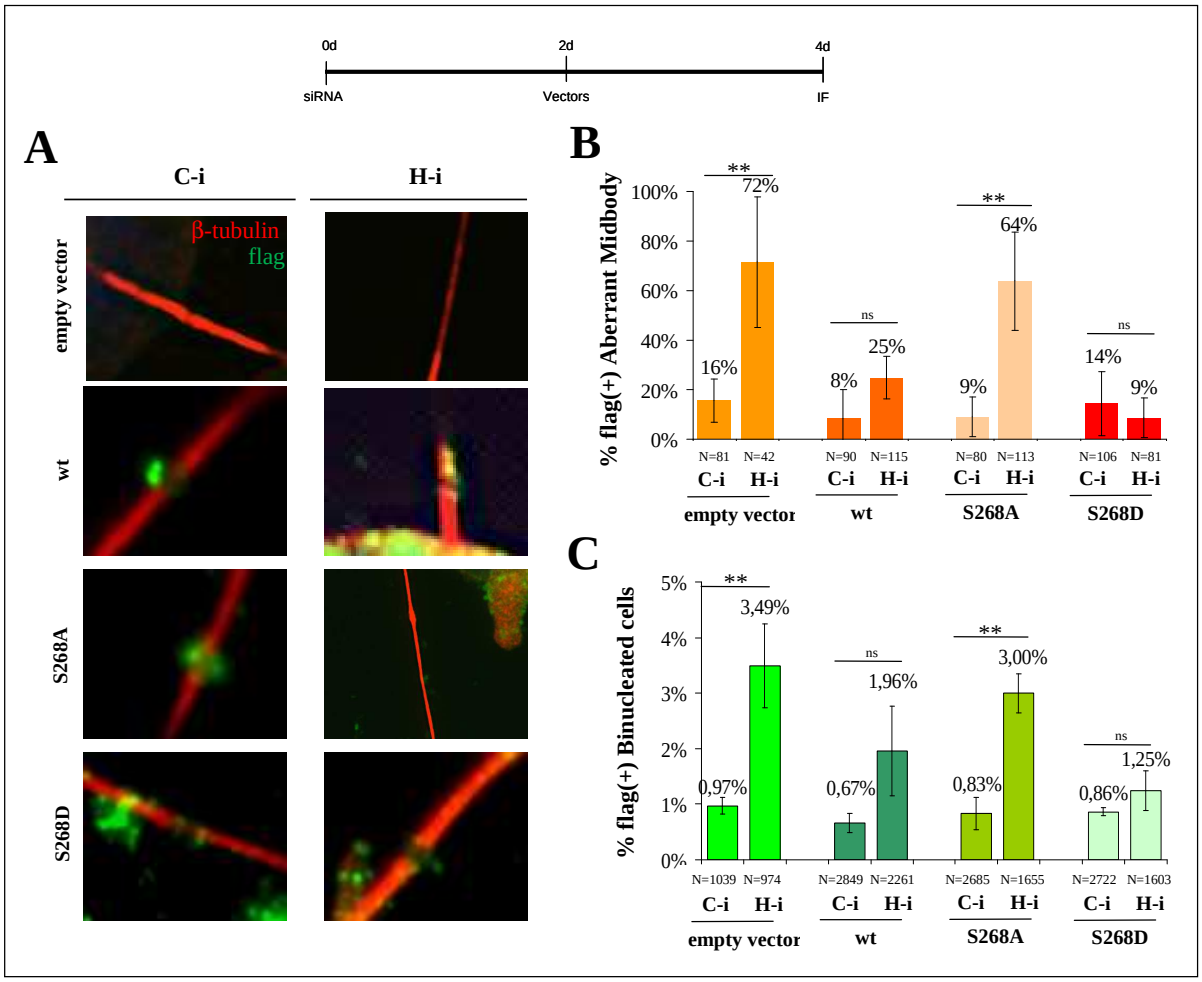


**Figure 34. Effects of spastin mutants over-expression in HIPK2-depleted cells.**
Upper: Schematic representation of RNAi followed by the plasmid transfection protocol. HeLa cells were transduced with control or HIPK2 siRNAs, transfected with indicated vectors as in Fig. 7 and analyzed by IF. (A) Representative merged IF images of indicated proteins in C-i and H-i cells (midbody magnifications are shown) stained with anti-flag Ab in green; anti β-tubulin Ab in red and Hoechst in blue. The percentage of flag aberrant midbodies (B) and of binucleated cells (C) in transfected cells (flag positive) are reported in the chart as mean±SD. N: number of analyzed flag positive aberrant midbodies or cells; ** $p<0.05$ t test Student.

During this analyzes, we reproducibly and consistently noticed that spastin S268A mutant staining was lower than those of spastin wt and S268D mutant in C-i and in H-i cells. To quantify this observation, we divided the staining of spastin positive cells into three classes based on signal intensity (i.e. +1, +2, and +3) and determined the percentage of cells in each class. As shown in the Fig. 24, spastin S268A over-expressing cells are mainly in the +1 and +2 staining classes, while spastin wt and S268D over-expressing cells are mainly in the +2 and +3 staining classes.

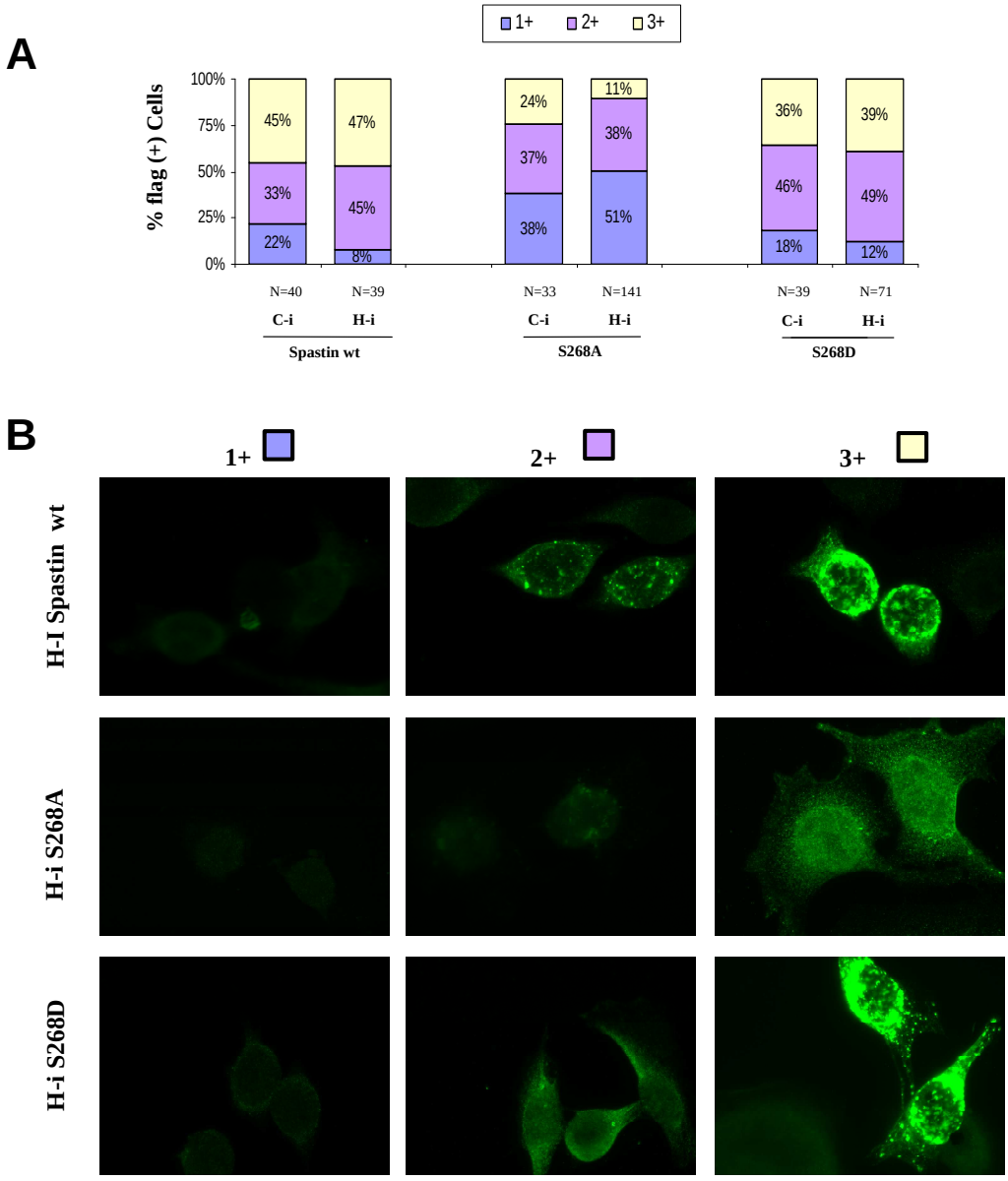


**Figure 35. Spastin mutants protein levels in C-i and H-i cells.**
C-i and H-i cells transfected with indicated vectors were subcategorized in three staining classes based on signal intensity. (A) The mean percentage of cells in the indicated classes are reported in the chart. (B) Representative IF images in each class stained with anti-flag Ab in H-i cells are shown. N: number of analyzed flag positive cells

Interestingly, when we evaluated the percentage of aberrant midbodies in each class of H-i cells, we observed that the aberrant midbodies are mainly in the +1 class and never in the +3 class and that this distribution is similar in all the spastin transfected cells independently from their S268 status (Fig. 36). This observation and the lowest staining levels of the S268A mutant (Fig. 35) led us to suppose that spastin S268A mutant is not able to rescue midbody aberrant phenotype because of its low levels in H-i cells.

In addition, although spastin wt, S268A and D mutants are able to localize at the midbody in C-i cells, we observed that only wt and S268D mutant are detectable at the midbody in the H-i cells (Fig. 34-A). Next, we analyzed transfected binucleated cells in H-i cells on the basis of the three staining classes (i.e. +1, +2, +3, as above) and we observed that binucleated cells are mainly in +1 and +2 classes and never in the +3 class. Accordingly to aberrant midbody distribution (Fig. 36), we found that the percentage of binucleated cells in each class is similar in all the spastin transfected cells independently from their S268 status (Fig. 36-B). These findings strongly suggest that spastin S268A mutant is not able to rescue cytokinesis defects in H-i cells because of its low levels.

Overall, we can conclude that these data support the hypothesis that HIPK2 regulates cytokinesis through spastin phosphorylation that is crucial to reach the spastin dosage required for abscission.

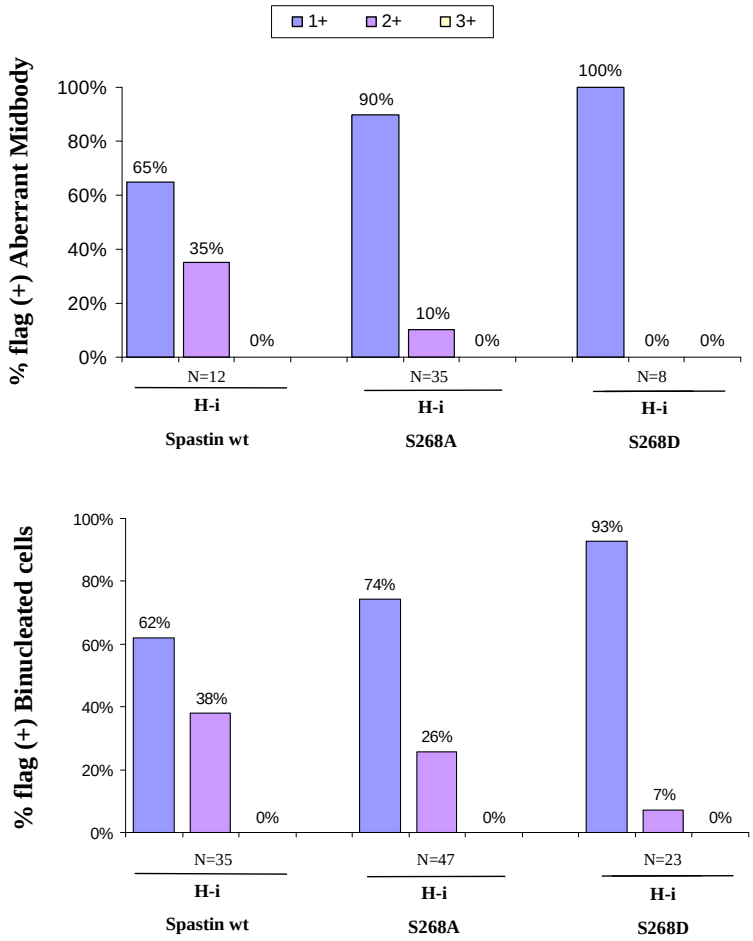


**Figure 36 Effects of different levels of spastin mutants in HIPK2-depleted cells.**
C-i and H-i cells transfected with indicated vectors were subcategorized in three staining classes based on signal intensity as in Fig. 34 and analyzed by IF. (A) The percentage of flag-positive aberrant midbody in indicated classes are reported in the chart as mean±SD. (B) The percentage of flag positive binucleated cells in indicated classes are reported in the chart as mean±SD. N: number of analyzed flag positive aberrant midbodies or cell.

# DUSCUSSION

To understand the cytokinesis role of the kinase HIPK2, we first evaluated which cytokinesis pathways are affected by HIPK2 depletion by analyzing the epistatic localization relationships of known cytokinesis components at the midbody in H-i cells. We observed that the cytokinesis master regulative kinases, the main factors involved in midzone/midbody stabilization and the ESCRT pathway-related abscission factors localize at the midbody in H-i as well as in C-i cells. However, we have noted that the examined abscission factors (i.e. Cep55, ALIX, and CHMP4B) appear to localize in a disorganized manner at the midbody in about half of the H-i analyzed cells compared to C-i cells, suggesting that HIPK2 depletion affected the abscission stage of cytokinesis. This observation is in agreement with the defects observed in HIPK2-depleted or null cells by IF and video Time-Lapse (Rinaldo et al., 2012; Valente et al., 2015; here in Fig. 7). Indeed, these cells do not show midbody formation/stabilization defects, while undergo to delayed abscission and cytokinesis failure. Interestingly, during our analysis the only factor that results absent at the midbody in a high percentage (37±4.9%) of H-i cells, is spastin, the MT severing ATPase essential for the last step of abscission (Connel et al., 2009). These data suggest that HIPK2 is involved in the abscission and might be relevant for the proper midbody localization of the abscission factors, in particular of spastin. In the process of controlling this possibly aberrant localization of spastin, we found that HIPK2 depletion results in a strong reduction of spastin protein levels. In particular, WB analyzes showed a drastic reduction of endogenous spastin in several murine and human tumour HIPK2-depleted cells, by using a mix of HIPK2 specific siRNAs, as well as by using each siRNA alone.

Furthermore, we showed that proteasome inhibition rescues spastin reduction in H-i cells, suggesting that spastin is regulated in a proteasome-dependent manner in HIPK2 depleted cells. It would be interesting to investigate whether polyubiquitination is a signal for spastin degradation and whether this modification is HIPK2-dependent. Interestingly, the lysine 554, a site common to all the spastin isoforms, was reported as a putative ubiquitinated site in a large scale screening combining MS with immunoenrichment of diglycine modified peptides (Wagner et al., 2012). It would be interesting to test whether K554 is polyubiquitinated in a HIPK2-dependent manner, non-ubiquitinatable K554R point

mutant isoforms could be generated and their resistance to HIPK2-mediated regulation be tested.

We demonstrated that HIPK2 directly regulates spastin protein levels in a phosphorylation dependent-manner, highlighting a novel mechanism of regulation of this MT severing enzyme. Until now, few studies have been carried out to investigate the mechanisms involved in the regulation of spastin. It has been demonstrated that spastin is regulated by NRF1 and SOX11transcriptional factor and by miR-96, miR-182 and Elk1 (Henson et al., 2012; Canbaz et al., 2011); however spastin post-translational regulation mechanisms are largely unknown. Interestingly, we identified HIPK2 as the first kinase that phosphorylates spastin in vitro and we assessed also the phosphorylation site by MS. Indeed, we found that HIPK2 phosphorylates spastin at Ser 268, a residue preceded by a proline, a consensus motif already reported for other HIPK2 targets (e.g. murine p53, Cecchinelli et al., 2006). Even if our analysis does not preclude the existence of other HIPK2 phosphorylation site/s, it is to be noted that the phosphorylation of this residue appear to be crucial for spastin protein levels regulation, as we showed by functional analyzing phospho-mimetic and not phosphorylatable S268 mutants, S268 D and A, respectively. In particular, we observed that S268A spastin mutant consistently show vey lower protein levels than wt and S268D, suggesting that the phosphorylation of this site is required for spastin stability. Since downstream effects mediated by HIPK2 kinase activity include also the control of target protein stability (Rinaldo et al., 2007a), it would be interesting to compare the stability of wt, non-phosphorylatable and phospho mimetic mutants by performing time course experiments in cells treated with cycloheximide to inhibit protein translation. To deeply characterize HIPK2 effects on spastin protein stability, it would be also relevant to measure the half-life of endogenous spastin isoforms in HIPK2 loss and gain of function experiments. In addition, we have planned to use the not phosphorylatable S268A mutant also to investigate whether HIPK2 phosphorylates spastin at other site/s, by using this mutant as substrate of HIPK2 in a kinase assay. Notably, cytokinesis defects were rescued by over-expressing wt spastin or a phosphomimetic S268D mutant in H-i cells. In contrast, no rescue was observed by over-expressing non-phosphorylatable spastin S268A mutant in H-i cells, maybe because of its low levels. Indeed, we observed that S268A mutant localize at the midbody only when it is present at high levels in the H-i cells (Fig. 37) and the rescue of the abscission defects appears to depend on exogenous spastin protein levels present in H-i cells. In agreement with these observations we observed that when we found exceptional S268A cells (i.e. in the +3

class) in H-i cells we observed that the MT of these midbodies are similar to those of C-i cells (Fig. 37), suggesting a rescue of aberrant midbody phenotype in these cells.

**Spastin v1 S268A in H-i cell**

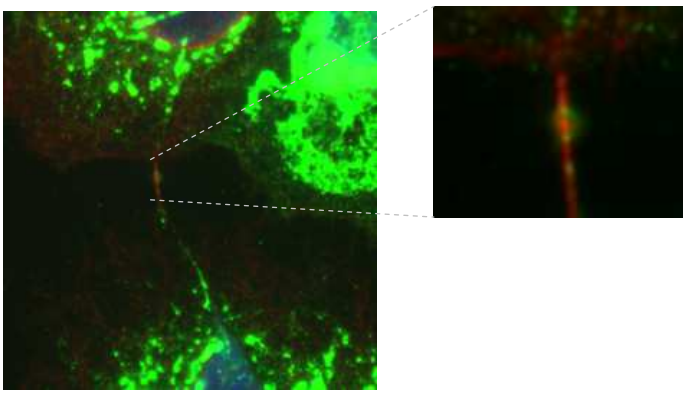

**Figure 37. H-i cells expressing high levels of spastin S268A mutant**
Representative merged IF image of spastin S268A high expressing cell (classified as +3) in H-i stained with anti-flag Ab in green; anti β-tubulin Ab in red and Hoechst in blue. Midbody magnification is shown.

These data led us to conclude that HIPK2 indirectly regulates cytokinesis through spastin phosphorylation, that is crucial to ensure the spastin dosage required for abscission. Furthermore, we demonstrated that the regulation of HIPK2 on spastin occurs downstream or independently from the phosphorylation of the extra-chromosomal H2B at S14.

Altogether, these findings support the following hypothetical working model (Fig. 38). In HIPK2-proficient cells: H2B is phosphorylated at S14, spastin is phosphorylated at S268 and its dosage is sufficient to cut MT midbody ensuring successful cytokinesis. In HIPK2 depleted cells: H2B is localized at the midbody but is not phosphorylated at S14, spastin is not phosphorylated at S268 and is degraded in a proteasome-dependent manner, thus its dosage is too low and the abscission fails. In this latter conditions, to over-express high levels of spastin do not affect H2B phosphorylation at S14 but can lead to MT cutting and successful cytokinesis. In HIPK2-deficient cells expressing H2B phospho-mimetic mutant, successful cytokinesis occurs independently from spastin too low dosage.

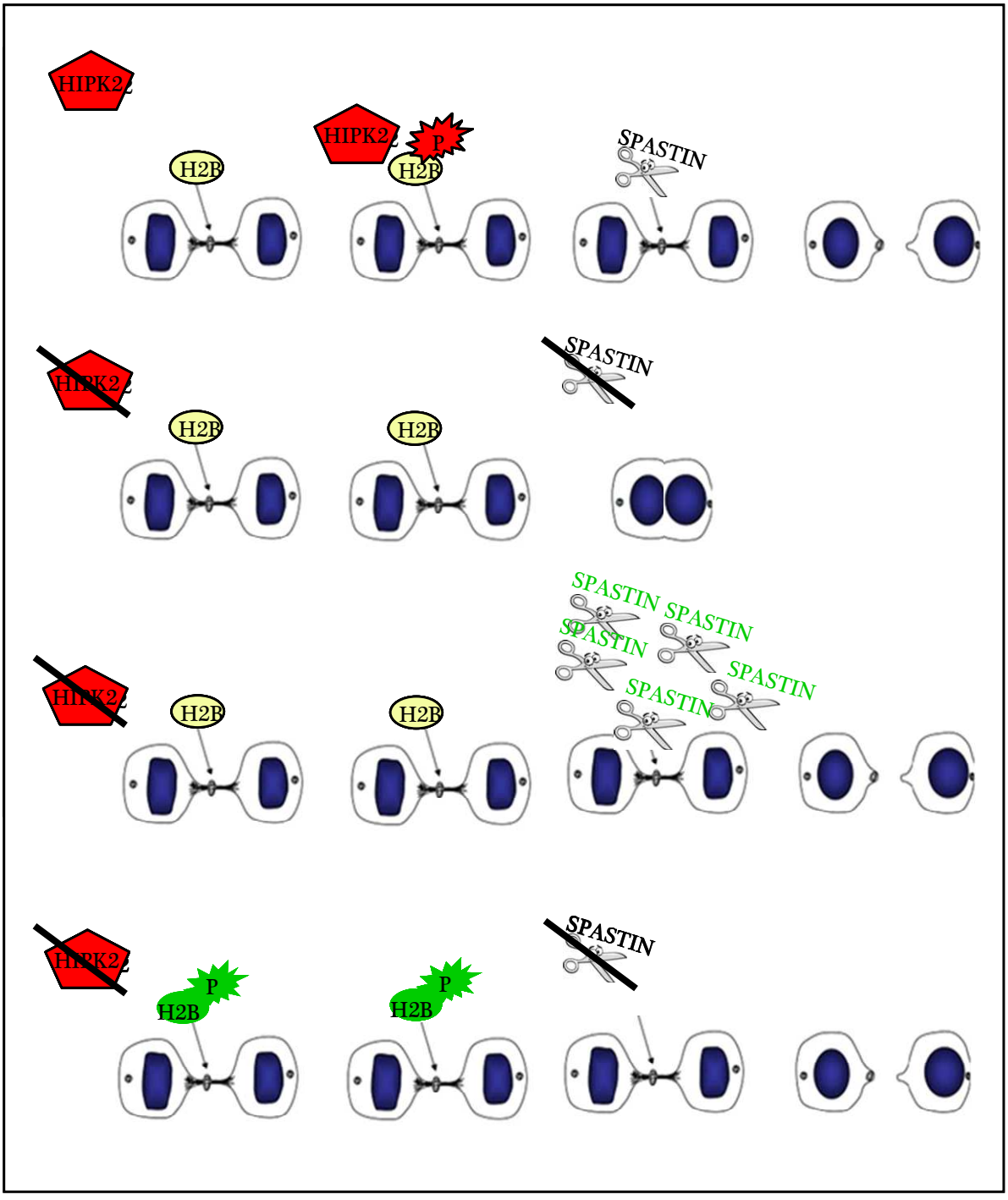


**Figure 38. Representation of a hypothetical working model for HIPK2, H2B and spastin cross-talk during cytokinesis**

In according to data reported in literature suggesting a relationship between midbody MT stability and cytokinesis defects (Sgro et al., 2015), we have preliminary data suggesting midbody MT hyper-stability in cytokinesis (Fig. 17). This phenomenon could be due to spastin low levels observed in H-i cells or to several other processes, such as for example alterations of the levels of the post-transcriptional modifications related to MT stability (i.e. tubulin acetylation and polyglutamylation). Although no alterations of these modifications were observed in H-i compared to C-i cells (data not shown), the spastin role and the mechanisms involved in the midbody MT hyper-stability observed in H-i cells remain to be investigated. Interestingly, we have data showing MT hyper-stability also in metaphase and interphase in H-i cells (data not show), suggesting that the MT hyper-stability might be a general phenomenon in H-i cells not only linked to MT midbody.

Since mutations in the SPG4 gene, encoding spastin, occurs in the most HSP case, the identification of a new pathway impinging on spastin regulation could have important implications for this motorneuronal disease, whose mainly molecular mechanism is the haploinsufficiency. Notably, we have evidence that HIPK2 regulates spastin levels also in motorneurons such as NSC-34 cells, as showed by HIPK2 loss/gain of function experiments (Fig. 22 and 28). Furthermore, we observed a strong reduction of endogenous spastin also in total protein lysates obtained from several brain regions of *Hipk2-/-* adult mice compared to those from *Hipk2* +/+ counterparts by WB (data not shown), suggesting that HIPK2 might regulate spastin in vivo. Recently, a gene-dosage rescue of neurite defects in SPG4 patients' neurons has been reported, providing the proof of principle that restoring physiological spastin levels might halt pathological phenotypes in patients (Havlicek et al, 2014). Since, precise levels of spastin appear crucial for its biological functions (Riano et al., 2009), our studies could open the way to evaluate whether manipulating HIPK2/spastin cross-talk might be a feasible therapeutic approach to restore spastin physiological levels in HSP patients. .

# MATERIALS AND METHODS

## Cells, virus and culture conditions

Human cervical adenocarcinoma HeLa cells and human lung adenocarinoma H1299 cells, were cultured in DMEM with low-glucose, supplemented with 10% heat-inactivated fetal bovine serum (FBS, Life Technologies, Carlsbad, CA, USA), 1% Penicillin-Streptomycin (Life Technologies, Carlsbad, CA, USA); while murine embryonal carcinoma p19 cells (kind gift from Dr. Soddu) were cultured in DMEM with high-glucose, supplemented with 7.5% heat-inactivated fetal bovine serum (FBS, Life Technologies, Carlsbad, CA, USA), 2.5% donor calf serum (DCS, Life Technologies, Carlsbad, CA, USA), 1% Penicillin-Streptomycin (Life Technologies, Carlsbad, CA, USA); and NSC-34 immortalized murine motorneurons (kind gift from Dr.Cozzolino) were cultured in DMEM-F12 1:1, supplemented with 10% heat-inactivated fetal bovine serum (FBS, Life Technologies, Carlsbad, CA, USA), 1% Penicillin-Streptomycin (Life Technologies, Carlsbad, CA, USA). These cellular lines were maintained in a humid incubator at 37°C in a 5% $CO_2$ environment. For live cell imaging, HeLa cells were cultured in DMEM medium without phenol red (Life Technologies, Carlsbad, CA, USA) supplemented with 10% heat-inactivated FBS and 2% Glutamax. Recombinant vaccinia virus vTF7-3 carrying the bacteriophage T7 gene 1, kindly provided by Dr. B. Moss, was propagated in HEK293 cells and used by standard techniques (as Rinaldo et al., 2012).

### RNA interference, RNA extraction and quantitative real-time RT-PCR

RNA interference was obtained in human cells by using commercially available HIPK2-specific stealth siRNA (a mix of four different siRNA in combination as in Rinaldo et al., 2012; Life Technologies, Carlsbad, CA, USA), spastin-specific siRNA and universal negative control stealth siRNA (Negative Medium GC Duplexes; Life Technologies, Carlsbad, CA, USA). RNAi was obtained in murine cells by using Hipk2 #3 siRNA that recognizes a sequence common to human and murine HIPK2. Cells were trasduced with 40 nM of HIPK2 siRNA and 20 nM of spastin siRNA using RNAi MAX reagent (Life

Technologies, Carlsbad, CA, USA) according to the instructions. The siRNAs sequences used are the following:

Hipk2 #1: CCCGAGUCAGUAUCCAGCCCAAUUU
AAAUUGGGCUGGAUACUGACUCGGG

Hipk2 #2: CCSCCSSCCUGACCAUGACCUUUAA
UUAAAGGUCAUGGUCAGGUUGGUGG

Hipk2 #3: GCCAAUCCCGAAGUCUCCAUACUAA
UUAGUAUGGAGACUUCGGGAUUGGC

Hipk2 #4: CAGGGUUUGCCUGCUGAAUAUUUAU
AUAAAUAUUCAGCAGGCAAACCCUG

Spastin: CCAGUGAGAUGAGAAAUAUUCGAUU
AAUCGAAUAUUUCUCAUCUCACUGG

In human cells Hipk2 specific RNAi was obtained also by transducing each HIPK2specific siRNA alone or by trasfecting plasmids expressing short hairpin RNA sequences ,such as pRetroSuper1376 , as reported in Cecchinelli et al., 2006)

RNA extraction and quantitative real-time RT-PCR were performed as in Iacovelli et al., 2009. The following primers were used:

Forward Hipk2 5′-AGGAAGAGTAAGCAGCACCAG-3′;

Reverse Hipk2 5′-TGCTGATGGTGATGACACTGA-3’;

Forward Actin 5′-CGATGCCCTGAGGCTCTTT-3′;

Reverse Actin 5′-TAGTTTCATGGATGCCACAGGAT-3′;

Forward spastin 5’-TCAGGCTGGTCTTGAACT -3’;

Reverse spastin 5’-ATGCATCTTCTGGCTGGG -3’;

Forward GAPDH 5’-TCCCTGAGCTGAACGGGAAG -3’;

Reverse GAPDH 5’-GGAGGAGTGGGTGTCGCTGT -3’.

Each target amplification was performed in duplicate on two different RNA preparations.

**Expression vectors and transfection**

The following plasmids were employed: EGFP-expressing vector (pEGFP-c2; Clontech, Mountain View, CA, USA); Flag- Empty Vector (Stratagene); pEGFP-HIPKwt, pEGFP-HIPK2-K221R, HA-Empty Vector, pET-HIPK2 HA,PET--HIPK2 K221A (Rinaldo et al., 2012). Spastin-1-turboGFP-tagged (RG220458, OriGene Technologies); Spastin-1-flag-myc-tagged (RC220458, OriGene Technologies): Spastin-2-flag-myc-tagged (RC214100,

OriGene Technologies); Spastin-1 plasmids express both M1 and M87 spastin isoforms; Spastin-2 plasmids express both M1DExon and M87DExon4 spastin isoforms. Cells were transfected by using Lipofectamine LTX and Plus reagent (Life Technologies, Carlsbad, CA, USA).

**Live-Cell imaging**

Cells were seeded in µ-slides 8-well (80826, Ibidi, Munchen, Germany) and observed under a Nikon Eclipse Ti inverted microscope using a Plane Apo 40x objective (Nikon). During the whole observation, cells were kept in a microscope stage incubator (Basic WJ, Okolab) at 37°C and 5% $CO_2$. DIC images were acquired every 4 minutes over a 26 hours period by using a DS-Qi1Mc camera. Image and video processing was performed with NIS-Elements AR 3.22 software (Nikon).

**Western blotting**

Total Cell Extracts (TCEs) were prepared in RIPA buffer [50mM Tris-HCl (pH 8), 600mM NaCl, 0.5% sodium deoxycholate, 0.1% SDS, 1% NP40 and 1mM EDTA] supplemented with protease and phosphatase inhibitors mix (Roche). Proteins were resolved by SDS-PAGE using NuPAGE® Novex Bis-Tris Gels 4-12%(Life Technologies, Carlsbad, CA, USA) or Bolt® Novex Bis-Tris Gels 4-12% ( Life Technologies, Carlsbad, CA, USA), transferred onto nitrocellulose membranes (Bio-Rad), and analyzed with the indicated antibodies (Abs). The following Abs were employed: anti-GAPDH (1:1000 diluition; Santa Cruz Biotechnology, Santa Cruz, CA, USA), anti-HIPK2 human (kindly provided by Dr. L. Shmidtz); anti-HIPK2 murine (1:1000 diluition; 2748-1, Epitomics); anti-GFP (1:500 diluition; Santa Cruz Biotechnology, Santa Cruz, CA, USA); anti-alpha-tubulin and anti-Actin (1:1000 diluition; Immunological Science, Rome, Italy); anti-Spastin (1:100 diluition; Santa Cruz Biotechnology, Sp 3G11/1, Santa Cruz, CA, USA); anti-GST (1:2000, kind gift by Dr Fanciulli), anti-HA (1:1000, Roche); anti-Flag Ab (1:1000 diluition; F7425, Rabbit, Sigma); anti-DDK (1:1000 diluition; TA50011, OriGene Technologies); anti-HRP-conjugated goat anti-mouse and anti-rabbit (Amersham, Piscataway, NJ, USA). Immunoreactivity was determined using the ECL-chemiluminescence or ECL-Prime reaction (Amersham, Piscataway, NJ, USA) following the manufacturer's instructions. Images acquisition and densitometric analysis was performed with Image Lab software (BIORAD).

## Immunofluorescence Microscopy

For immunofluorescence experiments, cells were seeded onto poly-L-lysine coated coverslips, fixed in 2% formaldehyde or in ice-cold methanol, washed three times in phosphate buffered saline (PBS), permeabilized in 0.25% Triton X-100 in PBS for 10 minutes, and then blocked in 5% bovine serum albumin (BSA) in PBS for 60 minutes before the required primary Abs was applied. For each employed Ab and IF condition see the table 1 (Tab. 1). Appropriate secondary FITC- or TRITC-conjugated Abs (Alexa-fluor, Invitrogene) were used. DNA was marked with HOECHST 33342 (Sigma).

**Table 1**: For each Ab are indicated all the tested compatible with midbody staining. F/P= Fix and Permeabilization were performed in combination as reported in Rinaldo et al., 2012. RT= Room Temperature; O/N=overnight.

| Ab | FIX | | | permeabilization | Diluition, time and temperature | |
|---|---|---|---|---|---|---|
| | Methanol 100% 5' -20°C | Formaldehyde 2% 10' RT | F/P | Triton 0,25% 10' RT | | |
| ALIX (Santa Cruz) | X | | | X | 1:100 2h Rt | Mouse |
| CEP55 (Santa Cruz) | | X | | X | 1:700 2h Rt | Mouse |
| AURORA-B (AIM1 bioscience) | | X | X | | 1:100 1h Rt | Mouse |
| INCENP (ABCAM) | | X | X | | 1:500 1h Rt | Mouse |
| SURVIVIN (epitomics) | | X | X | X | 1:100 1h Rt | Rabbit monoclonal |
| ECT-2 (Santa Cruz) | X | X | | X | 1:100 2h RT | Rabbit |
| PRC-1 (Santa Cruz) | X | X | | X | 1:100 2h RT | Rabbit |
| MKLP-1 (Santa Cruz) | X | X | | X | 1:100 2h RT | Rabbit |
| HIPK2 946 (Dr. Soddu's gift) | X | | | X | 1:50 O.N. +4°C in BSA 3% 0,1% TRITON | Rabbit |
| SPASTIN (Santa Cruz) | X | X | | X | 1:100 2 h RT | Mouse |
| PLK1 (Santa Cruz) | | X | | X | 1: 100 2h RT | Mouse |
| MgcRacGAp1 (ABCAM) | X | X | | X | 1:100 2h Rt or O/N +4°C | Goat |
| Citron kinase (Dr. Di Cunto's gift) | X 10 min | | | X | 1:100 2 h Rt | Mouse |
| CHMP4B (Santa Cruz ) | X | X | | | 1:100 2h RT | Rabbit |
| P-H2BS14 (Cell Signaling) | X | X | | | 1:100 2h RT | Rabbit |
| acetyl-tubulin (sigma) | | X | | X | 1:800 2h RT | Mouse |
| HA (roche) | | X | | X | 1:800 o/n +4°C | Mouse |
| Flag (policlonal sigma) | X | X | | X | 1:100 +4°C o/n or 2h RT | Rabbit |
| anti-α-tubulin FITC (Sigma). | X | X | | X | 1:300 1h 37°C | Mouse |
| anti-β-Tubulin-Cy3 (Sigma). | X | X | | X | 1:400 1h 37°C | Mouse |

Cells were examined under an Olympus BX53 microscope equipped with epifluorescence and photographs were taken (×100 objective) using a cooled camera device (ProgRes MF ). Cells were also analyzed using a Nikon Eclipse 90i microscope equipped with a Qicam Fast 1394 CCD camera (QImaging); image acquisition, deconvolution and Extended Depth of Focus on Z-serial optical sections were performed using Nis-Elements AR 4.2 (Nikon).

**Statistical analysis**

Significant changes were assessed by using Student's t test.

**In vitro Kinase Assay**

In vitro kinase assays were performed as in Rinaldo et al., 2012, by using different HIPK2 Kinase Domain (Kind gift of Dr. Savino (45kDa) or HIPK2 Active commercially available from Sigma (72 kDa) as enzymatic sources. In particular, since HIPK2 phosphorylates itself, we choose the opportune enzymatic source depending of its size in a manner to separate opportunely on the gel the enzymatic source and the substrate. The following recombinant proteins were employed: Spastin 79-278 aa= 6*His-SPASTIN (size:28 kDa, this protein was produced by Proteintech, catalogue number: ag18866, by expressing spastin 79-278 as 6xHis-tagged fusion protein in E. coli followed by Ni-sepharose purification); Spastin variant 1 and 2 - flag-myc-tagged proteins (size 60-65 KDa, these protein are produced by by OriGene, catalogue number, TP320458 and TP314100, respectively, by overexpression in HEK293 cells follwed by immunoprecipitation with anti-flag Ab) . Kinase assay was performed for 30 min at 30 °C in the following buffer: 20 mmHepes (pH 7.4), 50 mm NaCl, 10 mm MgCl2, 10 mmMnCl2) in the presence of 185 KBq [$\gamma^{32}$P]-ATP. The phosphorylated products were resolved on precast NuPAGE 4-12% gels and analyzed by autoradiography. MBP = myelin basic protein (Sigma-Aldrich, 25 Kda) was used as positive control. Gels were stained with Coomassie Blu (Sigma) to visualize protein.

**MS/MS identification**

In vitro kinase assays with cold ATP were performed as in Rinaldo et al., 2012, by using HIPK2 Kinase Domain Active commercially available from Sigma (72 kDa) as enzymatic sources and Spastin 79-278 aa= 6*His-SPASTIN as substrate. Kinase assay was performed for one hour at 30 °C in the following buffer: 20 mmHepes (pH 7.4), 50 mm NaCl, 10 mm MgCl2,

10 mmMnCl2) in the presence of cold ATP (Roche). Next, in collaboration with Dr Marco Crescenzi and Dr.ssa Serena Camerini at the Istituto Superiore di Sanità (ISS), we performed mass spectrometry (MS). The phosphorylated products were resolved on 1D-gel NuPAGE 4-12% (Novex, Invitrogen) run in morpholinepropanesulfoninic acid (MOPS) buffer and stained with the Colloidal Blue Staining kit (Invitrogen). The stained bands were cut from the gel and destained with a solution containing 50mM ammonium bicarbonate/acetonitrile (1:1 v/v) (CH3CN, Merck Darmstadt, Germany). Protein bands were subsequently subjected to cysteine reduction by 10 mM DTT for 1h at 56°C and alkylation by 50 mM iodoacetamide for 45min at RT in the dark, then dried in acetonitrile and finally in the speedvac apparatus. In gel digestion was performed by incubating gel particles with a solution containing 12.5 ng/ml trypsin (Promega, Madison, WI, USA) in 25 mM ammonium bicarbonate at 37°C over night under stirring. To recognize phosphorylated residues, peptide mixture was analyzed by nanoflow-reversed-phase liquid chromatography tandem mass spectrometry (RP-LC-MS/MS) using an HPLC Ultimate 3000 (DIONEX, Sunnyvale, CA U.S.A) connected on line with a linear Ion Trap (LTQ, ThermoElectron, San Jose, CA). Peptides were desalted in a trap-column (AcclaimPepMap100 C18, LC Packings, DIONEX) and then separated in a reverse phase column, a 10 cm long fused silica capillary (SilicaTipsFS 360-75-8, New Objective, Woburn, MA, USA), slurry-packed in-house with 5 μm, 200 Å pore size C18 resin (Michrom BioResources, CA). Peptides were eluted using a 30 min long linear gradient from 96% aqueous phase ($H_2O$ with 5% ACN, 0.1% formic acid) to 60% organic buffer (ACN with 5% $H_2O$ and 0.1% formic acid) at 300nl/min flow rate. Analyses were performed in positive ion mode with HV Potential set up around 1.7-1.8kV. The LTQ mass spectrometer operated in a data-dependent mode in which each full MS scan was followed by five $MS^2$ scans where the five most abundant molecular ions were dynamically selected and fragmented by collision-induced dissociation (CID) with a normalized collision energy of 35%. When a neutral loss (-49 or -32.6 Da) was detected among the three most abundant fragment ions in a $MS^2$ spectrum, a $MS^3$ spectrum was triggered. $MS^2$ and $MS^3$ spectra were matched searching for tryptic peptides coming from Spastin sequence through SEQUEST algorithm (Yates et al., 1995) incorporated in Bioworks software (version 3.3, Thermo Electron). Cysteine carbamidomethylation (Δm: +57 Da) was selected as static modification while methionine oxidation (Δm: +16 Da) and phosphorylation on tyrosine/serine/threonine residues (Δm: +80 Da) were taken in account as variable modifications. A peptide has been considered legitimately identified when it achieved cross correlation scores of 1.8 for [M+H]1+, 2.5 for[M+2H]2+, 3 for[M+3H]3+, and a probability cut-off for randomized identification of $p<0.001$.

**Enrichment in telophase cells**

HeLa cells were enriched in telophase by treatment with nocodazole (100ng/ml for 4 hours) followed by mitotic shake off, nocodazole wash-out and incubated for about 90 minutes to reach telophase stage.

**In vitro Binding assay, GST Pull-Down, and Co-immunoprecipitation**

For in vitro binding assay, recombinant eGST-HIPK2 and eGST-empty vector were produced in H1299 cells by infection with the vaccinia virus vTF7-3, followed by transfection with 2 μg of pcDNA3-eGST-HIPK2 or pcDNA3-eGST- empty vector plasmids using Lipofectamine LTX/plus (Invitrogen). TCEs were prepared 24 h post-transfection by incubation for 30 min at 4 °C in lysis buffer (50 mM Tris-HCl (pH 7.4), 300 mM NaCl, 5mM EDTA, 1%NP-40). After centrifugation, eGST-fusion proteins were purified from supernatant by overnight incubation with Glutathione-Sepharose 4 Fast Flow beads (GE Healthcare) at 4 °C. eGST-HIPK2 or eGST-empty vector bound to the beads were incubated with Spastin 79-278 His-tagged protein (described above; purchased by Proteintech) for 2 hours at room temperature in buffer phosphate (50mM TrisHCl, 5mM EDTA, 1% NP40) pH 7.5 with 75 mM NaCl, 150 mM NaCl or 225 mM NaCl. Pull-down GST-tagged proteins were washed three times with buffer phosphate and bound proteins were analyzed by WB.
For co-immunoprecipitation, protein G- Sepharose Beads (Ge-Healthcare) were blocked with BSA 1% and glycerol 7,5% at 4 °C for 1 hour, and thenincubated with anti-Flag-DDK Ab (Origene) at 4 °C for 1 hour. Proteins from tranfected cells were extracted by using non-denaturating Lysis Buffer [NDLB: 50mM Tris-HCl (pH 8), 150mM NaCl, 1% NP40 and 5mM EDTA] supplemented with protease- and phosphatase- inhibitor mix (Roche). TCEs were pre-cleared with Protein G- Sepharose Beads and then incubated over night at 4°C with Protein G Sepharose Beads conjugated with anti-Flag-DDK ab in NDLB. Beads were washed five times with NDLB and bound proteins analyzed by WB.

**Microtubules stability assay**

HeLa cells seeded onto poly-L-lysine coated coverslips and transduced with control or Hipk2-specific siRNA as described above. Four days after trasduction cells were treated with nocodazole 10 μM at 4°C to induce MT depolymerisation. Cells were fixed and processed for immunostaining with anti-tubulin abs at different time post treatment.

**Inhibitors treatment**

The following reagents were used: MG132 (Sigma), z-VAD-fmk (Calbiochem), DMSO (Sigma), and nocodazole (Sigma).

**Site-directed mutagenesis**

Site-directed mutagenesis of S268 to alanine (A) or aspartic acid (D) were performed by using QuikChange Lightning Supercharging Site-Directed Mutagenesis Kit (Agilent technologies) according to the manufacturer's instructions. PCR reactions for each single amino acid mutation were run for 18 cycles (see table 2). The resulting mutant plasmids were verified by DNA sequencing. The following primers were designed using QuikChange® Primer Design Program:

Forward spastin S268A

5′-AGGCCACCATAGAGCACCTGCTTACAGTGGTTTATCCATG-3′;

Reverse spastin S268A

5′-CATGGATAAACCACTGTAAGCAGGTGCTCTATGGTGGCCT-3';

Forward spastin S268D

5′-AGGCCACCATAGAGCACCTGATTACAGTGGTTTATCCATG-3′;

Reverse spastin S268D

5′-CATGGATAAACCACTGTAATCAGGTGCTCTATGGTGGCCT-3′

| cycles | temperature | time |
|---|---|---|
| 1 | 95°C | 2 min |
| 18 | 95°C | 50 sec |
| | 62°C | 50 sec |
| | 68°C | 7 min |
| 1 | 68°C | 7 min |
| | 4°C | ∞ |

# REFERENCES


Allison R, Lumb JH, Fassier C, Connell JW, Ten Martin D, Seaman MN, et al. An ESCRT-spastin interaction promotes fission of recycling tubules from the endosome. J Cell Biol; 202: 527–43. 2013

Anzilotti S, Tornincasa M, Gerlini R, Conte A, Brancaccio P, Cuomo O, Bianco G, Fusco A, Annunziato L, Pignataro G, Pierantoni GM. Genetic ablation of homeodomain-interacting protein kinase 2 selectively induces apoptosis of cerebellar Purkinje cells during adulthood and generates an ataxic-like phenotype. Cell Death Dis. Dec 3;6:e2004. 2015

Asthana J, Kapoor S, Mohan R, Panda D. Inhibition of HDAC6 deacetylase activity increases its binding with microtubules and suppresses microtubule dynamic instability in MCF-7 cells. J Biol Chem. 288(31):22516-26. 2013

Baas PW, Vidya Nadar C, Myers KA. Axonal transport of microtubules: the long and short of it. Traffic. 7(5):490-8. 2006

Bastos RN, Barr FA. Plk1 negatively regulates Cep55 recruitment to the midbody to ensure orderly abscission. J Cell Biol. 191(4):751-60. 2010.

Blackstone C. Cellular pathways of hereditary spastic paraplegia. Annu Rev Neurosci. 35:25-47. 2012.

Bracaglia G, Conca B, Bergo A, Rusconi L, Zhou Z, Greenberg ME, Landsberger N, Soddu S, Kilstrup-Nielsen C. Methyl-CpG-binding protein 2 is phosphorylated by homeodomain-interacting protein kinase 2 and contributes to apoptosis. EMBO Rep. 10, 1327-1333. 2009

Canbaz D, Kırımtay K, Karaca E, Karabay A. SPG4 gene promoter regulation via Elk1 transcription factor. J Neurochem. 117(4):724-34. 2011

Cecchinelli B, Lavra L, Rinaldo C, Iacovelli S, Gurtner A, Gasbarri A, Ulivieri A, Del Prete F, Trovato M, Piaggio G, Bartolazzi A, Soddu S, Sciacchitano S. Repression of the antiapoptotic molecule galectin-3 by homeodomain-interacting protein kinase 2-activated p53 is required for p53-induced apoptosis. Mol Cell Biol; 26:4746-57. 2006

Claudiani P, Riano E, Errico A, Andolfi G, Rugarli EI. Spastin subcellular localization is regulated through usage of different translation start sites and active export from the nucleus. Exp Cell Res; 309: 358–69. 2005

Connell JW, Lindon C, Luzio JP, and Reid E. Spastin couples microtubule severing to membrane traffic in completion of cytokinesis and secretion. Traffic 10:42–56. 2009.

Chun-Ting Chen, Heidi Hehnly, and Stephen J. Doxsey. Abscission: Orchestration of vesicle transport, ESCRTs and kinase surveillance. Nat Rev Mol Cell Biol. Nat Rev Mol Cell Biol; 13(8):483-8. 2012.

D'Avino PP, Capalbo L. Regulation of midbody formation and function by mitotic kinases. Semin Cell Dev Biol. pii: S1084-9521(16)30018-0. 2016.

D'Orazi G, Cecchinelli B, Bruno T, Manni I, Higashimoto Y, Saito S, Gostissa M, Coen S, Marchetti A, Del Sal G, Piaggio G, Fanciulli M, Appella E, et al. Homeodomain-interacting protein kinase-2 phosphorylates p53 at Ser 46 and mediates apoptosis. Nat Cell Biol 2002; 4:11-9.

D'Orazi G, Rinaldo C, Soddu S. Updates on HIPK2: a resourceful oncosuppressor for clearing cancer. J Exp Clin Cancer Res 2012; 31:63.

Elia N, Fabrikant G, Kozlov MM, and Lippincott-Schwartz J. Computational model of cytokinetic abscission driven by ESCRT-III polymerization and remodeling. Biophys. J. 102:2309–2320. 2012.

Elia N, Sougrat R, Spurlin TA, Hurley JH and Lippincott-Schwartz J. Dynamics of endosomal sorting complex required for transport (ESCRT) machinery during cytokinesis and its role in abscission. Proc. Natl. Acad. Sci. USA 108:4846–4851. 2011.

Errico A, Ballabio A, Rugarli EI. Spastin, the protein mutated in autosomal dominant hereditary spastic paraplegia, is involved in microtubule dynamics. Hum Mol Genet. 11(2):153-63. 2002

Errico A, Claudiani P, D'Addio M, Rugarli EI. Spastin interacts with the centrosomal protein NA14, and is enriched in the spindle pole, the midbody and the distal axon. Hum Mol Genet. 13(18):2121-32. 2004

Fededa, J.P., and Gerlich, D.W. Molecular control of animal cell cytokinesis. Nat. Cell Biol. 14:440–447. 2012.

Fonknechten N, Mavel D, Byrne P, Davoine CS, Cruaud C, Bönsch D, Samson D, Coutinho P, Hutchinson M, McMonagle P, Burgunder JM, Tartaglione A, Heinzlef O, Feki I, Deufel T, Parfrey N, Brice A, Fontaine B, Prud'homme JF, Weissenbach J, Dürr A, Hazan J. Spectrum of SPG4 mutations in autosomal dominant spastic paraplegia. Hum Mol Genet. 1;9(4):637-44. 2000

Ganem NJ, Pellman D. Limiting the proliferation of polyploidy cells. Cell.; 131:437-40. 2007

Guizetti J, Schermelleh L, Mäntler J, Maar S, Poser I, Leonhardt H, Müller-Reichert T, Gerlich DW. Cortical constriction during abscission involves helices of ESCRT-III-dependent filaments. Science. 25:331. 2011.

Havlicek S, Kohl Z, Mishra HK, Prots I, Eberhardt E, Denguir N, Wend H, Plötz S, Boyer L, Marchetto MC, Aigner S, Sticht H, Groemer TW, Hehr U, Lampert A, Schlötzer-Schrehardt U, Winkler J, Gage FH, Winner B. Gene dosage-dependent rescue of HSP neurite defects in SPG4 patients' neurons. Hum Mol Genet. 23(10):2527-41. 2014

Hazan J, Fonknechten N, Mavel D, Paternotte C, Samson D, Artiguenave F, Davoine CS, Cruaud C, Dürr A, Wincker P, Brottier P, Cattolico L, Barbe V, Burgunder JM, Prud'homme JF, Brice A, Fontaine B, Heilig B, Weissenbach J. Spastin, a new AAA protein, is altered in the most frequent form of autosomal dominant spastic paraplegia. Nat Genet. 23(3):296-303. 1999.

Henson BJ, Zhu W, Hardaway K, Wetzel JL, Stefan M, Albers KM, Nicholls RD. Transcriptional and post-transcriptional regulation of SPAST, the gene most frequently mutated in hereditary spastic paraplegia. PLoS One. 7(5):e36505. 2012

Hofmann TG, Moller A, Sirma H, Zentgraf H, Taya Y, Droge W, Will H, and Schmitz ML. Regulation of p53 activity by its interaction with homeodomain-interacting protein kinase-2. Nat Cell Biol 2002; 4:1-10

Hu CK, Coughlin M, and Mitchison TJ. Midbody assembly and its regulation during cytokinesis. Mol. Biol. Cell 23:1024–1034. 2012.

Hurley JH, Hanson PI. Membrane budding and scission by the ESCRT machinery: it's all in the neck. Nat Rev Mol Cell Biol. 11(8):556-66. 2010

Isono K, Nemoto K, Li Y, Takada Y, Suzuki R, Katsuki M, Nakagawara A, Koseki H. Overlapping roles for homeodomain-interacting protein kinases hipk1 and hipk2 in the mediation of cell growth in response to morphogenetic and genotoxic signals. Mol Cell Biol; 26:2758-71. 2006

Li XL, Arai Y, Harada H, Shima Y, Yoshida H, Rokudai S, Aikawa Y, Kimura A, Kitabayashi I. Mutations of the HIPK2 gene in acute myeloid leukemia and myelodysplastic syndrome impair AML1- and p53-mediated transcription. Oncogene; 26:7231-9. 2007

Kim YH, Choi CY, Lee SJ, Conti MA, Kim Y. Homeodomain- interacting protein kinases, a novel family of co-repressors for homeodomain transcription factors. J Biol Chem; 273:25875-79. 1998

Kim, EJ, Park JS, Um SJ. Identification and characterization of HIPK2 interacting with p73 and modulating functions of the p53 family in vivo. J Biol Chem; 277:32020-28. 2002

Krieghoff-Henning E, Hofmann TG. HIPK2 and cancer cell resistance to therapy. Future Oncol 2008; 4:751-4.

Lacroix B, van Dijk J, Gold ND, Guizetti J, Aldrian-Herrada G, Rogowski K, Gerlich DW, Janke C. Tubulin polyglutamylation stimulates spastin-mediated microtubule severing. J Cell Biol. 189(6):945-54. 2010

Lavra L, Rinaldo C, Ulivieri A, Luciani E, Fidanza P, Giacomelli L, Bellotti C, Ricci A, Trovato M, Soddu S, Bartolazzi A, Sciacchitano S. The loss of the p53 activator HIPK2 is responsible for galectin-3 overexpression in well differentiated thyroid carcinomas. PLoS One; 6:e20665. 2011

Lazzari C, Prodosmo A, Siepi F, Rinaldo C, Galli F, Gentileschi M, Bartolazzi A, Costanzo A, Sacchi A, Guerrini L, Soddu S. HIPK2 phosphorylates ΔNp63α and promotes its degradation in response to DNA damage. Oncogene Dec 1;30:4802-13. 2011

Lindsey JC, Lusher ME, McDermott CJ, White KD, Reid E, Rubinsztein DC, Bashir R, Hazan J, Shaw PJ, Bushby KM. Mutation analysis of the spastin gene (SPG4) in patients with hereditary spastic paraparesis. J Med Genet. 37(10):759-65. 2000

Mancuso G, Rugarli EI. A cryptic promoter in the first exon of the SPG4 gene directs the synthesis of the 60-kDa spastin isoform. BMC Biol; 6: 31. 2008

Mao JH, Wu D, Kim IJ, Kang HC, Wei G, Climent J, Kumar A, Pelorosso FG, DelRosario R, Huang EJ, Balmain A. Hipk2 cooperates with p53 to suppress γ-ray radiation-induced mouse thymic lymphoma. Oncogene; 31:1176-80. 2012

Mathieu J, Cauvin C, Moch C, Radford SJ, Sampaio P, Perdigoto CN, Schweisguth F, Bardin AJ, Sunkel CE, McKim K, Echard A, Huynh JR. Aurora B and cyclin B have opposite effects on the timing of cytokinesis abscission in Drosophila germ cells and in vertebrate somatic cells. Dev. Cell 26:250–265. 2013

Mishima M, Kaitna S, and Glotzer M. Central spindle assembly and cytokinesis require a kinesin-like protein/RhoGAP complex with microtubule bundling activity. Dev. Cell 2:41–54. 2002.

Mollinari C, Kleman JP, Jiang W, Schoehn G, Hunter T, and Margolis RL. PRC1 is a microtubule binding and bundling protein essential to maintain the mitotic spindle midzone. J. Cell Biol. 157:1175–1186. 2002.

Neto H and Gould GW. The regulation of abscission by multi-protein Complexes Journal of Cell Science 124: 3199-3207. 2011

Normand G and King RW. Understanding cytokinesis failure. Adv. Exp. Med. Biol. 676:27-55. 2010.

Petronczki M, Glotzer M, Kraut N, and Peters JM. Polo-like kinase1 triggers the initiation of cytokinesis in human cells by promoting recruitment of the RhoGEF Ect2 to the central spindle. Dev. Cell 12:713–725. 2007.

Puca R, Nardinocchi L, Givol D, D'Orazi G. Regulation of p53 activity by HIPK2: molecular mechanisms and therapeutical implications in human cancer cells. Oncogene; 29:4378-87. 2010

Reid E, Connell J, Edwards TL, Duley S, Brown SE, Sanderson CM. The hereditary spastic paraplegia protein spastin interacts with the ESCRT-III complex-associated endosomal protein CHMP1B. Hum Mol Genet; 14: 19–38. 2005

Riano E, Martignoni M, Mancuso G, Cartelli D, Crippa F, Toldo I, Siciliano G, Di Bella D, Taroni F, Bassi MT, Cappelletti G, Rugarli EI. Pleiotropic effects of spastin on neurite growth depending on expression levels. J Neurochem. 108(5):1277-88. 2009

Rinaldo C, Prodosmo A, Siepi F, Soddu S. HIPK2: a multitalented partner for transcription factors in DNA damage response and development. Biochem Cell Biol; 85:411-8. 2007

Rinaldo C, Prodosmo A, Mancini F, Iacovelli S, Sacchi A, Moretti F, Soddu S. MDM2- regulated degradation of HIPK2 prevents p53Ser46 phosphorylation and DNA damage-induced apoptosis. Mol Cell; 25:739-50. 2007

Rinaldo C, Moncada A, Gradi A, Ciuffini L, D'Eliseo D, Siepi F, Prodosmo A, Giorgi A, Pierantoni GM, Trapasso F, Guarguaglini G, Bartolazzi A, Cundari E, et al. HIPK2 controls cytokinesis and prevents tetraploidization by phosphorylating histone H2B at the midbody. Mol Cell 2012; 47:87-98.

Ritterhoff S, Farah CM, Grabitzki J, Lochnit G, Skurat AV, Schmitz ML. The WD40-repeat protein Han11 functions as a scaffold protein to control HIPK2 and MEKK1 kinase functions. EMBO J. 29:3750-3761. 2010

Roll-Mecak A1, McNally FJ. Microtubule-severing enzymes. Curr Opin Cell Biol. 22(1):96-103. 2010

Sanderson CM, Connell JW, Edwards TL, Bright NA, Duley S, Thompson A, et al. Spastin and atlastin, two proteins mutated in autosomal-dominant hereditary spastic paraplegia, are binding partners. Hum Mol Genet; 15: 307–18. 2006

Severson AF, Baillie DL, and Bowerman B. A Formin Homology protein and a profilin are required for cytokinesis and Arp2/3-independent assembly of cortical microfilaments in C. elegans. Curr. Biol. 12:2066–2075. 2002.

Sgrò F, Bianchi FT, Falcone M, Pallavicini G, Gai M, Chiotto AM, Berto GE, Turco E, Chang YJ, Huttner WB, Di Cunto F. Tissue-specific control of midbody microtubule stability by Citron kinase through modulation of TUBB3 phosphorylation. Cell Death Differ. 2015

Sharp DJ, Ross JL. Microtubule-severing enzymes at the cutting edge. J Cell Sci. 125(Pt 11):2561-9. 2012

Skop AR, Liu H, Yates J 3rd, Meyer BJ, Heald R. Dissection of the mammalian midbody proteome reveals conserved cytokinesis mechanisms. Science 305:61-66. 2004.

Soderblom C, Blackstone C. Traffic accidents: molecular genetic insights into the pathogenesis of the hereditary spastic paraplegias. Pharmacol Ther. 109(1-2):42-56. 2006

Solowska J, Garbern J, Baas PW. Evaluation of loss-of-function as an explanation for SPG4-based hereditary spastic paraplegia. Human Molec Genetics; 19: 2767–79. 2010

Solowska JM1, D'Rozario M, Jean DC, Davidson MW, Marenda DR, Baas PW. Pathogenic mutation of spastin has gain-of-function effects on microtubule dynamics. J Neurosci. 34(5):1856-67. 2014

Solowska JM1, Baas PW2. Hereditary spastic paraplegia SPG4: what is known and not known about the disease. Brain. 138(Pt 9):2471-84. 2015

Steigemann P, Wurzenberger C, Schmitz MH, Held M, Guizetti J, Maar S, Gerlich DW. Aurora B-mediated abscission checkpoint protects against tetraploidization. Cell 136:473-484. 2009

Steigemann, P., Gerlich, D.W. Cytokinetic abscission: cellular dynamics at the midbody. Trends Cell Biol. 19:606-616. 2009

Trotta N, Orso G, Rossetto MG, Daga A, Broadie K. The hereditary spastic paraplegia gene, spastin, regulates microtubule stability to modulate synaptic structure and function. Curr Biol. 14(13):1135-47. 2004

Valente D, Bossi G, Moncada A, Tornincasa M, Indelicato S, Piscuoglio S, Karamitopoulou ED, Bartolazzi A, Pierantoni GM, Fusco A, Soddu S, Rinaldo C. HIPK2 deficiency causes chromosomal instability by cytokinesis failure and increases tumorigenicity. Oncotarget. 6(12):10320-34. 2015

Wang Y, Debatin KM, Hug H. HIPK2 overexpression leads to stabilization of p53 protein and increased p53 transcriptional activity by decreasing Mdm2 protein levels. BMC Mol Biol; 2:8. 2001

Wee HJ, Voon DC, Bae SC, Ito Y. PEBP2-beta/CBF-beta-dependent phosphorylation of RUNX1 and p300 by HIPK2: implications for leukemogenesis. Blood; 112:3777-87. 2008

Wei G, Ku S, Ma GK, Saito S, Tang AA, Zhang J, Mao JH, Appella E, Balmain A, Huang EJ. HIPK2 represses beta-catenin-mediated transcription, epidermal stem cell expansion, and skin tumorigenesis. Proc Natl Acad Sci USA; 104:13040-5. 2007

White SR, Evans KJ, Lary J, Cole JL, Lauring B. Recognition of C-terminal amino acids in tubulin by pore loops in Spastin is important for microtubule severing. J Cell Biol. 176(7):995-1005. 2007

Wiggins AK, Wei G, Doxakis E, Wong C, Tang AA, Zang K, Luo EJ, Neve RL, Reichardt LF, Huang EJ. Interaction of Brn3a and HIPK2 mediates transcriptional repression of sensory neuron survival. J Cell Biol; 167:257-267. 2004

Yang D, Rismanchi N, Renvoisé B, Lippincott-Schwartz J, Blackstone C, Hurley JH. Structural basis for midbody targeting of spastin by the ESCRT-III protein CHMP1B. Nat Struct Mol Biol. 15(12):1278-86. 2008.

Yu W, Qiang L, Solowska JM, Karabay A, Korulu S, Baas PW. The microtubule-severing proteins spastin and katanin participate differently in the formation of axonal branches. Mol Biol Cell. 19(4):1485-98. 2008

Zakharenko S1, Popov S. Dynamics of axonal microtubules regulate the topology of new membrane insertion into the growing neurites. J Cell Biol. 143(4):1077-86. 1998

Zhang Q, Yoshimatsu Y, Hildebrand J, Frisch SM, Goodman RH. Homeodomain interacting protein kinase 2 promotes apoptosis by downregulating the transcriptional corepressor CtBP. Cell 2003; 115:177-86.

Zhang Q and Wang Y. Homeodomain-interacting protein kinase-2 (HIPK2) phosphorylates HMGA1a at Ser-35, Thr-52, and Thr-77 and modulates its DNA binding affinity. J. Proteome Res. 6:4711-4719. 2007

Zhu C, Lau E, Schwarzenbacher R, Bossy-Wetzel E, Jiang W. Spatiotemporal control of spindle midzone formation by PRC1 in human cells. Proc Natl Acad Sci USA. 103(16):6196-201. 2006.